KINEMATICS AND ENERGETICS OF ANNA'S HUMMINGBIRDS (*CALYPTE ANNA*) PERFORMING HOVERING FLIGHT IN GROUND EFFECT, ASCENDING AND DESCENDING VERTICAL FLIGHT, AND FORWARD FLIGHT IN AN ASYMMETRIC FLOW

by

Erica J. Kim

A dissertation submitted in partial satisfaction of the

requirements for the degree of

Doctor of Philosophy

in

Biophysics

in the

Graduate Division

of the

University of California, Berkeley

Committee in charge:

Professor Robert Dudley, Chair
Professor Robert J. Full
Professor Mimi Koehl
Professor Philip Marcus

Fall 2014

Abstract

KINEMATICS AND ENERGETICS OF ANNA'S HUMMINGBIRDS (*CALYPTE ANNA*) PERFORMING ASCENDING AND DESCENDING VERTICAL FLIGHT, HOVERING FLIGHT IN GROUND EFFECT, AND FORWARD FLIGHT IN AN ASYMMETRIC FLOW

by

Erica J. Kim

Doctor of Philosophy in Biophysics

University of California, Berkeley

Professor Robert Dudley, Chair

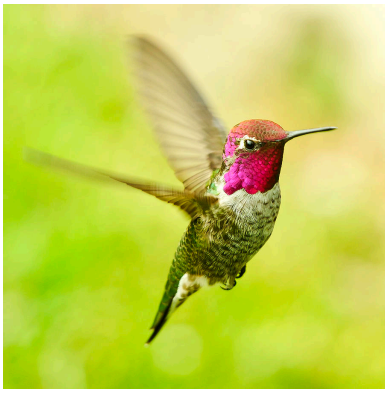

Anna's Hummingbird (*Calypte anna*) [photo credit: Edmund Wu]

Hummingbirds are exceptional among vertebrates in their extreme flight capabilities. They are unique in their ability to not only sustain hovering flight, but also to fly backwards, dive at high speeds, and perform quick alternations in flight speed and body orientation. Such capabilities require hummingbirds to have large metabolic power reserve, mechanical power output, force production, and maneuverability. These features, along with the relative ease of working with hummingbirds in a laboratory setting, make them a particularly convenient model system to assess different aspects of flight mechanics. Hence, this thesis is broadly on the flight performance of Anna's hummingbirds (*Calypte anna*) (seen in the above figure), a hummingbird species found year-round on the University of California, Berkeley campus, with each chapter focusing on a different flight mode: hovering flight in ground effect (chapter 1), vertically ascending steady flight (chapter 2), vertically descending steady flight (chapter 3), and forward flight in an asymmetric flow (chapter 4). The overall goal of each chapter is to gain a greater understanding of the aforementioned flight modes (e.g. what are the kinematic correlates of each flight mode, or what are the limits that constrain such a flight

mode), all of which have not been previously analyzed in any detail. The primary results of each chapter are as follow:

CHAPTER 1: Aerodynamic performance and energetic savings for flight in ground effect are theoretically maximized during hovering, but have never been directly measured for flying animals. This study evaluated flight kinematics, metabolic rates and induced flow velocities for Anna's hummingbirds hovering at heights (relative to wing length R=5.5 cm) of 0.7R, 0.9R, 1.1R, 1.7R, 2.2R and 8R above a solid surface. Flight at heights less than or equal to 1.1R resulted in significant reductions in the body angle, tail angle, anatomical stroke plane angle, wake-induced velocity, and mechanical and metabolic power expenditures when compared with flight at the control height of 8R. By contrast, stroke plane angle relative to horizontal, wingbeat amplitude and wingbeat frequency were unexpectedly independent of height from ground. Qualitative smoke visualizations suggest that each wing generates a vortex ring during both down- and upstroke. These rings expand upon reaching the ground and present a complex turbulent interaction below the bird's body. Nonetheless, hovering near surfaces results in substantial energetic benefits for hummingbirds, and by inference for all volant taxa that either feed at flowers or otherwise fly close to plant or other surfaces.

CHAPTER 2: Kinematic measurements of Anna's hummingbirds hovering within a vertical wind tunnel operated at different downward airspeeds enabled assessment of their climbing flight. With increasing climbing speed, body posture became more vertical while both flapping frequency and stroke amplitude increased substantially. Climbing flight at 4 m s^{-1} was close to the upper limit for sustained vertical ascent, and is the highest relative climb speed reported among vertebrates. Estimates of mechanical power output for the flight muscles ranged from 114 W kg^{-1} in free hovering to 293 W kg^{-1} and 341 W kg^{-1} for climbing at 4 m s^{-1}, depending on how body drag was estimated. These values, along with associated kinematic responses, differ from those estimated in other studies of maximum flight performance in hummingbirds (i.e., load lifting and hovering in hypodense air). Depending on the particular context of maximum aerodynamic demand, a variety of changes in wingbeat kinematics may be used to increase lift and power production. Our results suggest that male Anna's hummingbirds ascend vertically in the course of their courtship displays at maximum sustained speeds possible.

CHAPTER 3: Kinematic and metabolic measurements of Anna's hummingbirds hovering within a vertical wind tunnel operated at different upward airspeeds enabled assessment of their steady (i.e. zero acceleration) vertical descending flight. With increasing descent speed, body posture became more horizontal, and stroke amplitude decreased substantially while flapping frequency increased slightly. Metabolic power decreased substantially, from 49 ml O_2 g^{-1} hr^{-1} in hovering to 31 ml O_2 g^{-1} hr^{-1} and 23 ml O_2 g^{-1} hr^{-1} for descending at 3 m s^{-1} and 4 m s^{-1}, respectively. Estimates of mechanical power decreased concurrently, resulting in either no significant change in muscle efficiency or a slight decrease in efficiency, from 11% in hovering to 9% and 7% in 3 and 4 m s^{-1} descent speeds, respectively. The increase in flapping frequency, accompanied by the increases in the standard deviations of both flapping frequency and stroke amplitude,

suggests that the primary challenge to sustaining steady high-speed descent is in the maintenance of position control and stability.

CHAPTER 4: This study assessed the detailed three-dimensional kinematics of Anna's hummingbirds performing forward flight in both a uniform velocity field with average airspeed of 9.8 m s^{-1}, and a spatially asymmetric velocity field in which one wing was immersed in a 4.2 m s^{-1} speed airflow while the other wing was immersed in a 10.8 m s^{-1} speed airflow. Hummingbirds were able to maintain stable flight in the asymmetric flow field easily, without any learning or prior training. In the uniform flow, wing kinematics were bilaterally symmetric. In the asymmetric flow condition, by contrast, there were significant differences between wing variables, with the greatest differences found in the mid-downstroke chord angle and the mid-downstroke angle of attack, with no significant rolling or yawing of the body as well. Our results demonstrate how hummingbirds are able to redirect aerodynamic force vectors without having to concurrently reorient their body position. More specifically, hummingbirds are able to utilize small changes in wing angle of attack to generate the substantial aerodynamic force asymmetries required for stable flight within the asymmetric flow.

All housing and experimental protocols were approved by the Institutional Animal Care and Use Committee at the University of California, Berkeley. Bird captures were carried out under permits from the United States Fish and Wildlife Service and the California Department of Fish and Game.

TABLE OF CONTENTS

LIST OF SYMBOLS

A_{front}	projected area of the body onto the XY-plane
$C_{d,par}$	parasitic drag coefficient
D_{par}	parasitic drag force
g	gravitational constant (9.81 m s^{-1})
k	induced velocity correction factor
m	body mass
n	wingbeat frequency
IGE	"in ground effect"
OGE	"out of ground effect"
P_{ind}	muscle mass-specific induced power
P_{input}	muscle mass-specific metabolic power (equal to P_{met})
P_{mech}	total muscle mass-specific mechanical power (equal to P_{total})
P_{met}	muscle mass-specific metabolic power (equal to P_{input})
P_{PE}	muscle mass-specific potential energy power
P_{par}	muscle mass-specific parasitic power
P_{pro}	muscle mass-specific profile power
P_{total}	total muscle mass-specific mechanical power (equal to P_{mech})
ΔP	excess power increment
R	winglength
Re_b	Reynolds number of the body
U_r	relative wing velocity
v_h	hovering induced velocity
v	non-hovering induced velocity
V	vertical climb velocity
$\dot{V}_{O_2}$	oxygen consumption rate (units: ml O_2 g^{-1} hr^{-1})
α	angle of attack
α_c	chord angle
β_a	anatomical stroke plane angle (angle between stroke plane and body vector)
β_h	stroke plane angle (angle between stroke plane and horizontal plane)
γ	body angle
η	muscle efficiency
θ	deviation angle
φ	position angle
Φ	wing stroke amplitude
Φ_{hor}	wing stroke amplitude, projected onto the horizontal plane
χ	tail angle
ρ	air density

LIST OF FIGURES AND TABLES

ACKNOWLEDGEMENTS

I am grateful for the funding provided by an NSF Integrative Graduate Education and Research Traineeship (IGERT) from UC Berkeley's Center for Interdisciplinary Biological Inspiration in Education and Research (CiBER), as well as additional funding from UC Berkeley's Biophysics Graduate Program.

Additionally, I would like to thank members of the Dudley Lab, the UC Berkeley Biophysics program, and the greater Biomechanics community at UC Berkeley in general, for support and fellowship, without which this dissertation could not have been completed.

CHAPTER 1

HOVERING PERFORMANCE OF ANNA'S HUMMINGBIRDS

IN GROUND EFFECT

Introduction

Flying near the ground or near any other boundary can potentially influence aerodynamic performance (Leishman, 2006; Johnson, 1980; Norberg, 1990; Rayner, 1994). In this so-called ground effect, interaction between the vortex wake generated in flight and the lower boundary reduces the mean induced velocity, and thus both the induced and total powers required to hover (Rayner and Thomas, 1991). Lighthill (1979) pointed out that reduction of the induced velocity can be viewed as an interaction between the vortex wake generated by the wings and an opposing vortex structure actuated by the ground via a mirroring effect. Whereas the aerodynamic advantages of forward locomotion in ground effect have been modeled for birds (Withers and Timko, 1977; Finn et al., 2012; Rayner, 1991), little brown bats (Aldridge, 2009) and flying fish (Park and Choi, 2010) (see also Blake, 1979; Webb, 2002; Nowroozi, et al., 2009), the actual mechanical as well as metabolic consequences of such flight have yet to be systematically characterized. These advantages would be expected to be maximal for hovering, based on the associated power savings experimentally found for helicopters flying close to the ground (Leishman, 2006; Johnson, 1980; Rayner and Thomas, 1991).

In comparison with rotor aircraft, relatively little is known about the vortex wake for animals hovering in ground effect. Flow visualization of the helicopter wake in ground effect indicates a reduction in the axial descent speed of the tip vortices, along with wake compression and lateral expansion of these vortices as they approach the ground (Light, 1993) (for geometrical details, see Figure 5.35 of Leishman, 2006). Computational analyses for simple insect models and simulations of two-dimensional aerofoils hovering in ground effect suggest similar vortex structures (Pereira, et al., 2009; Gao and Lu, 2008). However, given the three-dimensional complexities of flapping wings, it is possible that the associated vortex wakes generated during ground effect for animals differ from those predicted theoretically. Furthermore, if and how animals change their kinematics in response to ground proximity is not clear, owing to the somewhat inconsistent results found within the literature. For example, hovering mandarin fish increase their fin stroke amplitude while in ground effect (Blake, 1979); by contrast, plaice in forward swimming decrease tailbeat amplitude and frequency, whereas swimming cod do not make any changes at all (Webb, 2002). For volant taxa, the effects of ground distance on flight kinematics and power expenditure are particularly unresolved.

Although hummingbirds rarely hover near the ground, they often feed from flowers surrounded by other vegetational surfaces; this can potentially induce a ground

effect if the air transmissivity of the foliage matrix is low. More importantly, hummingbirds can serve to illustrate general biomechanical patterns that pertain to other nectarivorous taxa (e.g. many insects, bats and other nectarivorous birds) which commonly hover above leaves and floral structures, as well as predatory hymenopterans and much smaller parasitoids which fly near the ground or over larvae either on or within leaves. Because hummingbirds represent a particularly convenient model system with which to assess the mechanics of flight in ground effect, given the ease with which they hover in laboratory contexts as well as the feasibility of measuring their metabolic rates during various aerodynamic tasks (Chai and Dudley, 1995; Chai and Dudley, 1996; Ortega-Jiménez and Dudley, 2012), we seek here to characterize wing and body kinematics, mechanical power expenditures, metabolic rates and wake-induced velocities for Anna's hummingbird (*Calypte anna*) hovering both in ground effect and out of ground effect. We predict that hummingbirds hovering in ground effect will decrease their induced velocity without any concurrent changes in wing kinematics, in comparison with control flight.

Materials and methods

Four male Anna's hummingbirds (mean body mass m±1$s.d.$: 4.7 ± 0.2 g (range of 4.5 – 5.0 g)) were trained to hover-feed within a Plexiglas cube (90 × 90 × 90 cm). A syringe filled with a 20% solution of Nektar-Plus (Nekton GmbH, Pforzheim, Germany) and tipped with a respirometry mask was placed within the cube's center (Figure 1.1a). A transparent Plexiglas platform (61 × 77 cm), which served as a ground surface, was positioned at variable distances beneath the syringe. The ground height h, defined here as the perpendicular distance between this platform and the center of the respirometry mask, was altered by moving the platform up or down along the vertical z-axis. Six values of h were used in experiments, corresponding to heights of 0.7R (4 cm), 0.9R (5 cm), 1.1R (6 cm), 1.7R (9 cm), 2.2R (12 cm) and 8R (43 cm), where R was the average wing length (5.45 ± 0.05 cm) for the four experimental hummingbirds. Treatment orders were selected randomly to minimize any order bias. Heights lower than 0.7R were not tested, as physical contact between birds and the platform (via either the feet or the tail) frequently occurred. The maximum ground distance of 8R served as the control treatment. As distances between the syringe and the chamber's walls were typically 7 – 8 wing lengths in all cases, aerodynamic effects of sidewalls were assumed to be insignificant, according to a theoretical analysis of the recirculation effects for animal fliers within a confined volume (see Figure 4 in Rayner and Thomas, 1991).

Flight kinematics and energetics

At each of the aforementioned height treatments, each bird was filmed three times (mean video duration was five wingbeats, corresponding to about 0.11 s of film) during the course of an experimental trial. We used two synchronized high-speed video cameras (X-PRI, AOS Technologies AG, Baden Daettwil, Switzer- land), recording at 1000 frames s^{-1} (800 × 600 pixels), positioned above and laterally to the hovering bird (figure 1a). Three-dimensional calibrations and digitization were carried out in Proanalyst (Xcitex Inc.). For each video frame, marked coordinates of the right wing tip, right shoulder, rump, center tail tip and neck (Figure 1.1b) were digitized and imported into

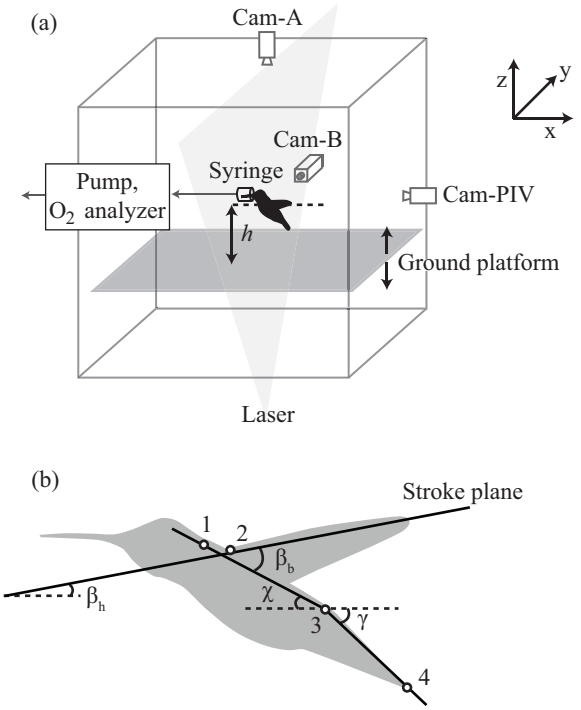

Figure 1.1. (a) Experimental configuration for kinematic, metabolic, and PIV measurements (note that these measurements were made separately on any given bird, not simultaneously). The global coordinate system as well as positions of the syringe, moving platform, high-speed cameras ("Cam-A" and "Cam-B"), pull-through respirometry system, and PIV system (laser sheet and "Cam-PIV") are labeled. (b) Landmarks for the bird's neck (1), right shoulder (2), rump (3), and tail tip (4), angles for the stroke plane and anatomical stroke plane (β_h and β_b, respectively), and body and tail angle (χ and γ, respectively) are also indicated. A positive tail angle denotes that the vector between rump and tail tip point is oriented below the (x,y) plane, whereas a negative tail angle denotes that the vector is oriented above this plane.

Matlab (v. 7.8.0.347). We calculated the stroke plane by finding the best-fit plane, based on principal component analysis, for positions of the wingtip and shoulder points throughout the course of each video. We subsequently calculated body angle χ, tail angle γ, horizontal stroke plane angle β_h, anatomical stroke plane angle β_a (see Tobalske et al., 2007), stroke amplitude Φ and wingbeat frequency n with custom Matlab code, where, using the coordinate system as depicted in figure 1a, we defined χ, γ, and β_h as the acute angles between the XY-plane and the stroke plane, the vector from neck to rump and the vector from rump to tail tip, respectively, and β_a as the sum of β_h and χ. We estimated the flapping frequency n (i.e. angular frequency/2π) from a sinusoidal curve fit using the bird's wingtip z-coordinate positions as a function of time. Wingbeat amplitude Φ was estimated by measuring the average angle formed by the wingtip at the start of each downstroke, the shoulder and the wingtip at the end of the downstroke. Horizontal and anatomical stroke plane angles were calculated for only three birds; because of a low shutter speed used in the lateral video recordings for one individual, lateral tracking of the wingtip was difficult and thus omitted. Kinematic variables for each bird were averaged over the three separate video sequences, yielding a total of 60 wing beats per treatment (four birds × three video sequences per bird × five wingbeats per video sequence) for estimates of x, g, F and n, and a total of 45 wing beats per treatment (three birds × three video sequences per bird × five wingbeats per video sequence) for estimates of β_a and β_h.

The metabolic power input (P_{met}) during hover-feeding was estimated from measurements of the rate of oxygen consumption via the use of a pull-through mask respirometry system (Bartholomew, 1986). As the birds hovered and fed, expired gas was first drawn into the respirometry mask (fashioned from the tip of a 10 ml plastic syringe) at a rate of 1200 ml O_2 min^{-1}, water-scrubbed with Drierite (W. A. Hammond Drierite Co. Ltd), and then passed into an O_2 analyzer equipped with a flow meter (FOXBOX-C field gas analysis system, Sable Systems International). A photoresistor-LED circuit, modeled after that of Bartholomew & Lighton (1986), indicated the presence of the bird's head within the mask, thereby enabling accurate measurements of feeding duration. As all of the hummingbirds fed for relatively short durations (mean of 4.98 s), oxygen consumption rates infrequently reached steady-state values. We therefore estimated the oxygen consumption rate by dividing the total volume of depleted O_2 by the total summed feeding time, using only those feeding bouts with durations greater than 2 s in our analysis (Bartholomew and Lighton, 1986; Welch, 2011). Because hummingbirds had unlimited access to the sugar-dense Nektar-Plus solution, we used a respiratory quotient of one (Suarez et al., 1986) and an energy conversion factor of 21.1 J ml^{-1} O_2 (Brobeck and Dubois, 1980) for subsequent metabolic calculations. A mean of 12 metabolic measurements were made for each bird per treatment over a period of 3 days.

Total mechanical power output, assuming perfect elastic storage, P_{mech} (Ellington, 1984), was calculated for three birds as the sum of the profile power P_{pro} and the induced power P_{ind}, where P_{ind} and P_{pro} correspond to the rates of energy expenditure required to generate vertical force, and to overcome both form and skin friction drag of the wings, respectively. We estimated P_{ind} as the product of the weight and the induced velocity v_h, where v_h was explicitly measured, as described below. We estimated P_{pro} following

Ellington (1984), but used the values of induced velocity that we directly measured for calculations. We additionally used a profile drag coefficient of 0.139 based on the drag measurements made on a revolving hummingbird wing at *Re* of 5000 and angle of attack of 158 (see Figure 5 from Altshuler et al., 2004), rather than estimating the coefficient based on wing mean Reynolds number (Ellington, 1984). This approach does not capture the variation in profile drag deriving from changes in angles of incidence associated with variable flow fields, but is intended here as a first approximation for comparison with induced power estimates. Muscle efficiency η was estimated as the ratio of mechanical power output to metabolic power input, with the added assumption that only 90% of the metabolic power was expended by the flight muscles (Morris et al., 2010).

Vortex wake visualization and quantification

Smoke visualization technique was used to obtain qualitative details of the vortex wake for one hummingbird. A separate wire cube structure (30 × 30 × 30 cm) with a Plexiglas floor was covered at the top and all sides with mesh fabric. A syringe containing Nektar-Plus was placed within the cube, either at 0.9R (5 cm) above the floor to resemble in ground effect conditions, or at 2.2*R* (12 cm) above the floor to simulate out of ground effect conditions. Owing to the porous nature of the mesh walls and top, we assumed that the only aerodynamic effect of the cube on the hummingbird's wake came from the solid ground surface. To visualize the airflow, a water-based, non-toxic smoke (American DJ ecowater-based fog juice) generated by a smoke machine (Eliminator E119 FOGIT) was forced into the cube from above. To reduce the initially high flow rate (approx. 100 m^3 min^{-1}), four layers of mesh were used as a filter to laminarize flow and to reduce the rate by one to two orders of magnitude.

A continuous 200 mW laser (532 nm Spyder II GX, Wicked Lasers) with a quartz cylindrical optic illuminated the fog along the dorsal plane of the hummingbird's wake, whereas a video camera (Sony HDR-UX1, 1440 × 1080) oriented orthogonally to the laser sheet recorded the flow field at 120 frames s^{-1}. Video sequences of the hummingbird hover-feeding were then de-interlaced using the program AVIDEMUX, yielding an effective filming speed of 240 frames s^{-1}.

For three hummingbirds, particle imaging velocimetry (PIV) was used to quantitatively characterize their vortex wakes at each height treatment. Birds were first trained for several days to hover- feed in the aforementioned Plexiglas flight cube in a low-light environment. For PIV experiments, the cube's interior was seeded approximately 20 s prior to filming with a cloud of volatilized olive oil droplets (approx. 1 mm in diameter) generated by a LaVision vaporizer at a rate of approximately 1.4 × 10^{10} particles s^{-1}. The vaporizer was positioned at the open side door to the flight cube; this door was closed following seeding to minimize any subsequently induced flows which in any event would be insignificant relative to the convection generated by hummingbird wing motions. We illuminated these volatilized oil droplets using a 2 mm thick laser sheet in the transverse plane just behind the trailing edge of the wing (approx. 0–2 cm from the wingroot), using a double pulsed 50 mJ Nd:YAG laser (532 nm New Wave Research SoloPIV) running at a pulse repetition rate of 15 Hz. An Image ProX CCD camera (1600 × 1200 pixels), synchronized with and positioned perpendicular to

the laser sheet, was used to capture sequences of 24 pair-wise images (dt=100 ms) over an approximately 15 × 20 cm^2 area. The camera was equipped with a 52 mm f/1.8D Nikon lens with the aperture set at 1.8. We used LaVision DAVIS software (v. 7.2.1.76) with multi-pass correlation (128 × 128 and 32 × 32, 50% overlap) to process images and to derive particle displacements. Images were then post-processed using a peak ratio deletion (Q<1.3), a median vector filter that removed vectors larger than twice the neighbouring r.m.s. velocity, and a single 3 × 3 smoothing average.

From all of the recorded PIV sequences, 100 images were chosen for each bird at each height treatment. In order to consistently obtain images in which the vortex wake was unmistakably identifiable across all treatments, we analyzed the wake only during the mid-downstroke phase of the wingbeat. To estimate the potential error introduced by this selection bias, we also made 25 measurements of the far wake velocity w for an entire wingbeat, for three birds at the control height. We measured w in the region between the wing edge and 4 cm beneath each of the wings, at a position between the wingtip and root vortices. As there was no significant difference between PIV measurements for the left and right wings' wakes, estimates of wake velocities were averaged for the two sides. The induced velocity was then calculated as v_h=0.5w in accordance with momentum theory (Leishman, 2006; Johnson, 1980).

Statistical analysis

Repeated measures ANOVA was performed for each of the dependent variables χ, γ, βh, βa, Φ, n, P_{mech}, P_{met}, v_h, and η, using distance from ground as the independent variable (i.e. a within- subjects factor). Tukey's post hoc tests were then carried out to deter- mine statistically significant differences among treatments. All parameters fulfilled both normality conditions (Shapiro – Wilk test, p<0.05 for all cases) and equality of variance (Bartlett's tests, p<0.05 for all cases). A Huynh – Feldt correction was applied to variables in which sphericity was violated (i.e. p<0.05 for Mauchly's test). We also used a Kruskal – Wallis test to determine if our in ground effect/out of ground effect ratios for mechanical and metabolic power expenditure were comparable to values predicted by two theoretical models for helicopters (Cheeseman & Bennett's model, and Hayden's model; see Leishman, 2006). All statistical tests were carried out in R v. 2.10.1 (R Development Core Team).

Results

Repeated measures ANOVAs indicated significant differences with ground height in body angle (F=14.5, d.f.=5,15, p=2.3×10^{-4}) (Figure 1.2B), tail angle (F=14.9, d.f.=5,15, p=1.6×10^{-3}) (Figure 1.2B, Table 1.2), anatomical stroke plane angle (F=11.1, d.f.=5,10, p=0.012) (Figure 1.2C), metabolic power (F=14.3, d.f.=5,15, p=5.5×10^{-4}) (Figure 1.3A), induced velocity (F=48.5, d.f.=5,10, p=3×10^{-3}), and mechanical power (F=37.9, d.f.=5,10, p=8.7×10^{-6}) (Figure 1.3B). By contrast, no significant variation with ground height was found for the horizontal stroke plane angle (F=2.7, d.f.=5,15, p=0.2) (Figure 1.2C), wingbeat frequency (F=1.5, d.f.=5,15, p =0.8) (Figure 1.2A), and stroke amplitude (F=0.4, d.f.=5,15, p =0.3) (Figure 1.2A). Post-hoc tests indicated that hummingbirds

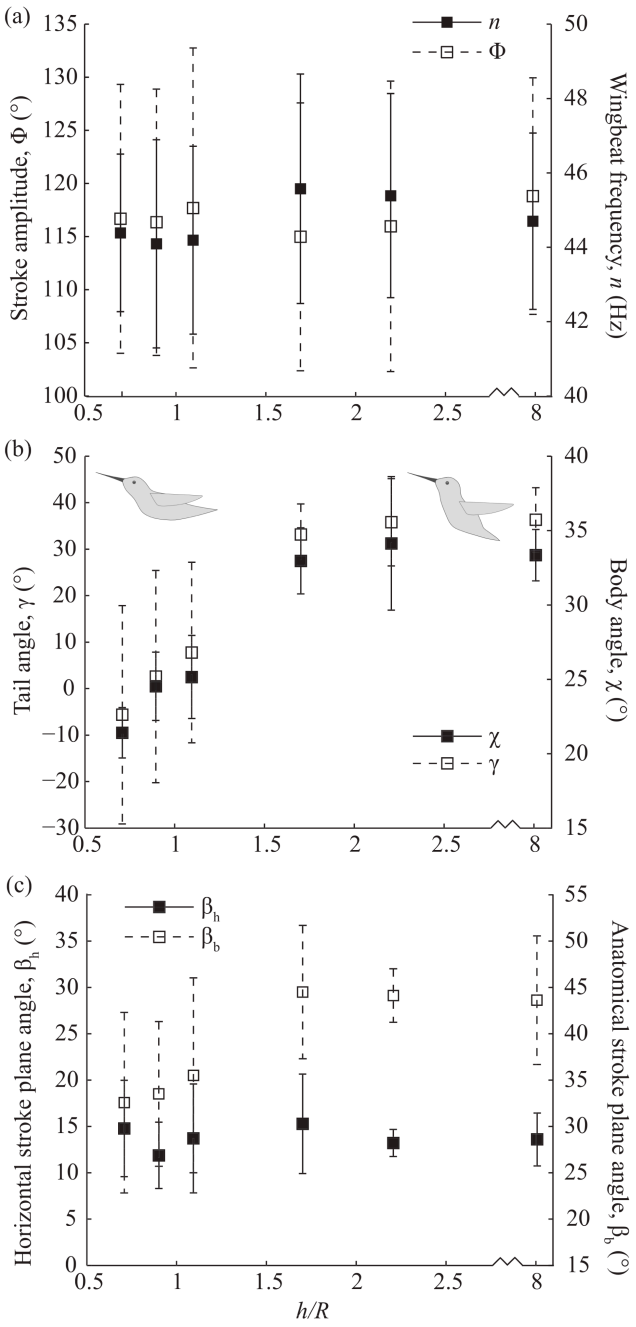

Figure 1.2. (a) Stroke amplitude Φ and wingbeat frequency n; (b) tail angle γ and body angle χ; (c) horizontal stroke plane angle β_h and anatomical stroke plane angle β_b, all as functions of the normalized ground distance (h/R). Data are presented as mean values ±1 s.d., with N=4 for all variables except β_h and β_b, for which N=3.

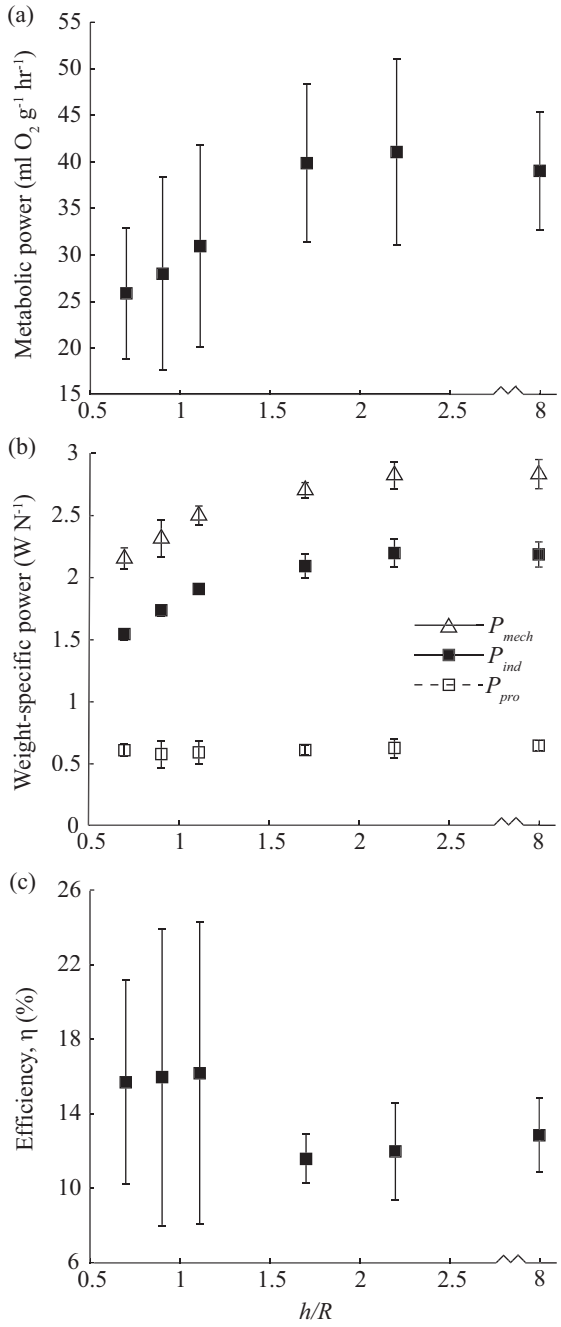

Figure 1.3. (a) Metabolic rate, (b) Body-weight specific profile power, induced power, and total mechanical power; and (c) efficiency, all as functions of the normalized ground distance (h/R). Data are presented as mean values ±1 s.d., with N=4 for metabolic rates and N=3 for all other data.

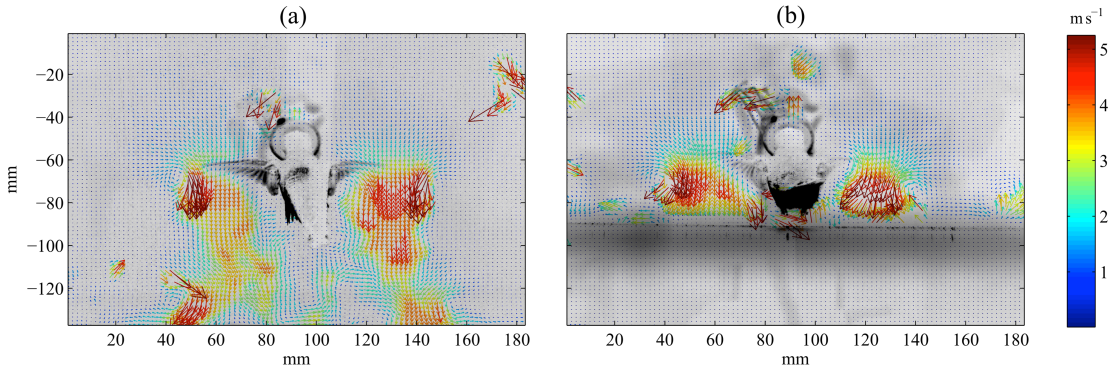

Figure 1.4. PIV vector fields for a hummingbird hovering IGE at 4 cm (a) and OGE at 9 cm (b) from the ground.

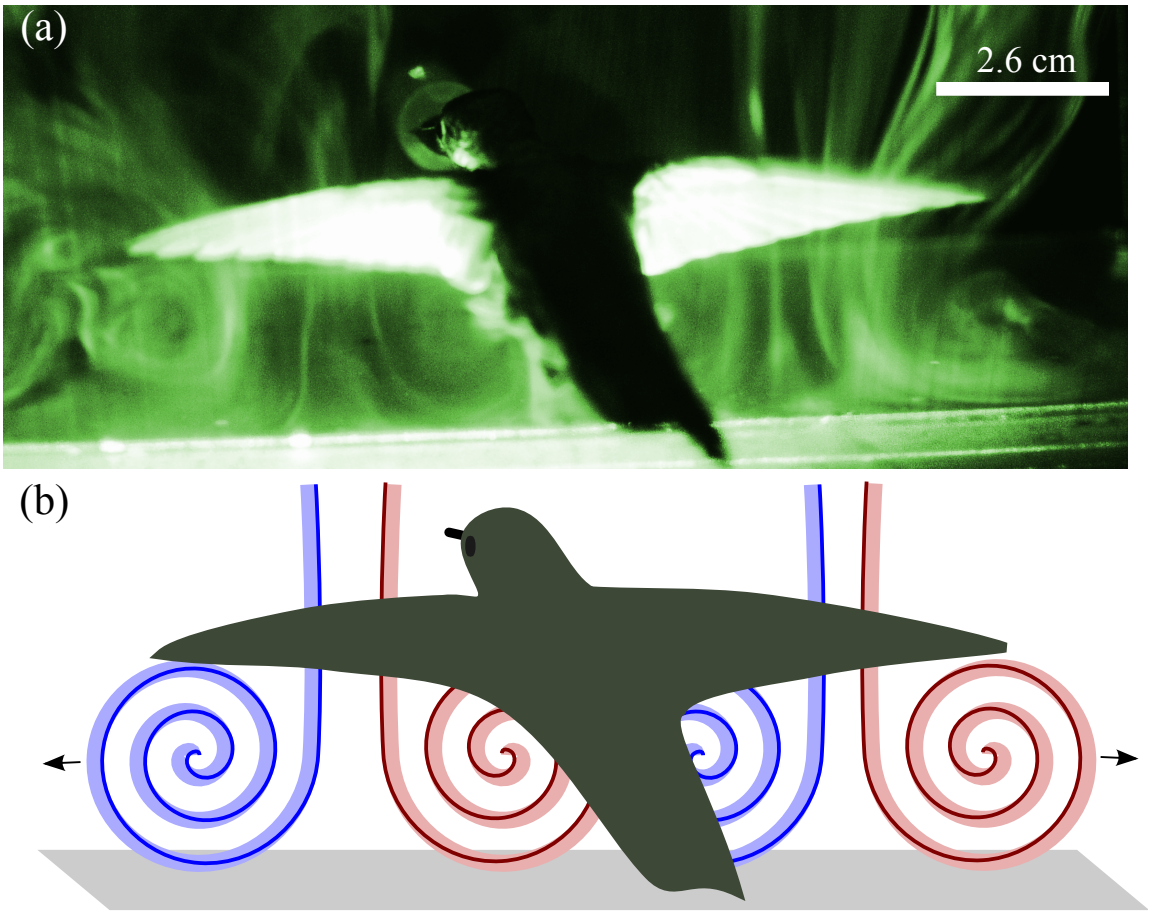

Figure 1.5. Smoke visualization of the hummingbird's hovering wake in ground effect at 5 cm: (a) raw video frame and (b) stylized reconstruction highlighting primary wake structures. White arrows indicate vortex translation, whereas blue and red lines indicate clockwise and anticlockwise motions of the vortex, respectively.

hovering at ground distances equal to 0.7R, 0.9R, and 1.1R (but not at 1.7 or 2.1 R) exhibited significantly lower values of χ, β, P_{met}, v_h, and P_{mech} than at the control height of 8R.

Maximal reductions in P_{met}, v_h, and P_{mech} due to the ground effect were 34%, 29%, and 24%, respectively. Whereas there was a 5% increase in flight muscle efficiency at h/R=0.7, 0.9, and 1.1 compared with the control height, this difference was not statistically significant (F=1.39, d.f.=5,10, p=0.36) (Figure 1.3C). We found that w measured during mid-downstroke gives values 15% higher than when measured for the entire stroke (two-way Anova; F=167.6, d.f.=1,149, $p=2\times10^{-16}$). In contrast, we found no significant differences among birds (two-way Anova; F=0.86 d.f.=2,148, p=0.4). We also found no significant differences between IGE/OGE ratios for either mechanical and metabolic power and the predicted values derived from Chesseman-Bennet and Hayden's models (Kruskal-Wallis test, χ^2=1.1, df= 4, p=0.89).

Both PIV results and smoke visualization of the bird's wake revealed vortex rings derived from each wing during both up- and downstroke. However, visual clarity of these vortex ring pairs was substantially better defined during the downstroke (Figure 1.4). Qualitative observations revealed that, during hovering at h=2.2R, the two vortex rings descended axially and eventually dissipated, with relatively minimal mutual interaction. During hovering at h=0.9R, however, the rings shed from each wing interacted both with the ground surface and with one another. Although this interaction resulted in a highly complicated three-dimensional flow pattern, certain repeated phenomena were observed (Figure 1.5). Upon impacting the ground, each vortex was stretched laterally and thus asymmetrically. The innermost sides of the paired rings collided with one another beneath the hummingbird's body, and rolled upwards in a turbulent flow maintained by subsequent pairs of shed vortex rings. The outer edges of the paired rings, by contrast, appeared to travel along the ground away from the bird.

Discussion

Hummingbirds experienced substantial reductions in both mechanical and metabolic power expenditure (by up to 24% and 34%, respectively) when hovering at heights less than 1.7R above the ground (Figure 1.3b). The magnitude of these reductions is comparable, at equivalent relative ground heights, to previously published theoretical estimates for helicopters hovering in ground effect (Leishman, 2006; Johnson, 1980; Cheeseman and Bennett, 1955; Hayden, 1976) (Figure 1.6). Reductions in the mechanical power found for hummingbirds were also broadly similar to those (15–25%) calculated for mandarin fish hovering in water at comparable fin lengths above a surface (Blake, 1979). Whereas these fish concurrently decreased fin stroke frequency and increased fin stroke amplitude while in ground effect (Blake, 1979), there were no significant changes in n and Φ for the hummingbirds in this study. Experimental evidence from a flapping robotic wing suggests that beetles during takeoff increase lift production by up to 18% at a ground height of 0.5R (Truong et al, 2013). Moreover, a three-dimensional computational fluid dynamics simulation of a fruit fly hovering at a height of 0.8R shows increases in vertical forces by up to approximately 9% compared with those generated

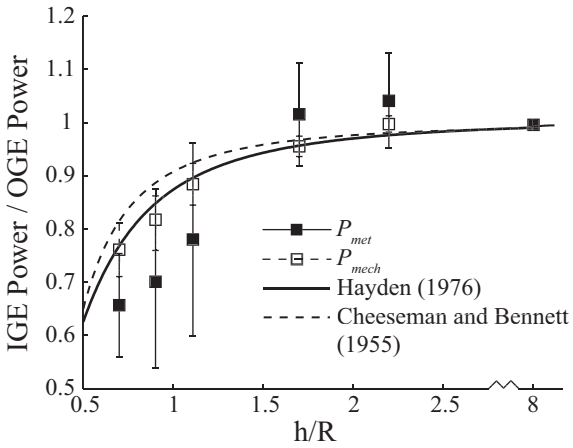

Figure 1.6. Comparison of average weight-normalized mechanical power estimates for Anna's Hummingbirds with theoretical estimates derived from two helicopter models for hovering in ground effect (IGE) and out of ground effect (OGE) (Cheeseman and Bennett, 1955; Hayden, 1976; as cited in Leishman, 2006; Johnson, 1980), with vertical thrust assumed to be constant. P_{met}: black squares; P_{mech}: open squares; Hayden's model: broken line; and Cheeseman-Bennett's model: continuous line. Error bars correspond to ±1 s.d. (N=3).

out of ground effect (Maeda and Liu, 2013). For hummingbirds flying in ground effect, rollup of the innermost edges of the generated vortex rings created a region of relatively continuous upwash directly beneath the bird's body; this flow, termed the 'fountain effect' (Maeda and Liu, 2013), could underlie the observed postural changes observed in hummingbirds and may be generally relevant to in ground effect flight.

For helicopters hovering in ground effect with constant vertical force (as opposed to hovering with constant power), reduction in the downwards induced velocity yields an effective decrease in aerodynamic angles of attack (Leishman, 2006), reducing blade pressure and total power expenditure. Qualitatively, we observed no substantial changes in the geometrical angle of attack for hummingbirds flying in ground effect and out of ground effect, although small changes may nonetheless ensue and, given typical nonlinearity in the lift polar for animal wings at low angles of attack, result in significant changes in profile drag and associated power. However, trends in total power expenditure are largely driven by the relatively large magnitude of induced power with respect to the profile power (Figure 1.3b). Profile power (assuming a constant drag coefficient of 0.139) represents only 20–25% of total power, but if the profile drag out of ground effect is increased, via an assumed increase in mean angle of attack (because of a reduced induced velocity), it would decrease the correlation between mechanical and metabolic power (Figure 1.3a,b). On the contrary, assuming a decreased profile drag in ground effect will reduce the modest estimates of profile power even further, and will only marginally change the aforementioned correlation as total power is driven primarily by the trend in induced power. Relevant unsteady drag data for hummingbird wings flapping at different angles of attack are in any event unavailable, but we consider the overall mechanical power trends derived here to be reliable, given the dominant role of the induced power component. Thus, we found full support for our initial predictions, based on helicopter theory, that the induced velocity decreases while the wing kinematics remain unchanged, with respect to ground height, for hovering hummingbirds.

In contrast to wingbeat kinematics, both body and tail angles changed significantly with ground height, with hummingbirds adopting a more horizontal body posture when hovering in ground effect compared with out of ground effect (Figure 2b). Although all hummingbirds in this study decreased their tail angle in ground effect, the relative extent of such reduction varied considerably among individuals, resulting in large standard deviations in γ at $h/R \leq 1.1$ (Figure 1.2b). Some individuals occasionally allowed either their tail or feet to touch the ground while hover-feeding at the lowest heights (such cases were excluded from the analyses presented here); other individuals, however, appeared to keenly avoid contacting the ground surface, exhibiting negative tail angles as large as $\gamma = -30°$. Body angle changes mirrored those in tail angle, such that x and g changed con- currently. It is well known that aircraft in ground effect experience pitch instability, which is usually corrected by a highly elevated tail plane in order to shift the center of pitch downstream while maintaining the aerodynamic center of height upstream (for details, see Rozhdestvensky, 2000). Altshuler et al. (2009) proposed that hummingbirds use their tails to deflect the flow created by the wings in order to maintain pitch stability (see also Su et al., 2012 for use of tail in pitch recovery by a passerine bird). Changes in body angle might thus necessitate a concomitant change in tail angle in

order to effect stability in pitch. Equivalently, of course, an externally imposed change in tail angle would require alteration of body angle.

Alternatively, a change in body posture could reflect the obvious differences between in ground effect and out of ground effect hovering in the overall surrounding flow. For a rotorcraft hovering in ground effect, the wake first descends axially, impacts the ground surface and then subsequently undergoes lateral expansion (Nathan and Green, 2012). Smoke visualizations of rotors hovering in ground effect also reveal a region of stagnant fluid in the center of the wake (Nathan and Green, 2012; Fradenburgh, 1960). We observed a similar effect in hummingbirds, except that the wings shed pairs of vortices (Figure 1.5a), rather than the single helical wake of rotors or the hypothesized single vortex previously described for hovering hummingbirds (Warrick et al., 2005). Recent PIV studies have shown that the near wake generated by a hummingbird during hovering is composed of two distinct vortex rings (Pournazeri et al., 2013; Wolf et al., 2013). The rollup of the innermost edges of the rings created a region of relatively continuous upwash directly beneath the bird's body (see also Maeda and Liu, 2013), which was qualitatively observed but not quantified in this experiment. This flow, termed the 'fountain effect' (Maeda and Liu, 2013), could underlie the observed postural changes observed in hummingbirds and may be generally relevant to in ground effect flight. As the model used here for estimating mechanical power did not take into account this potentially beneficial phenomenon, P_{mech} could be overestimated, resulting in the higher (albeit statistically insignificant) muscle efficiency values found for birds hovering in ground effect relative to out of ground effect (Figure 1.3c).

Additionally, we found a high interindividual variance in efficiency estimates for flight in ground effect, driven mostly by mass-specific rates of oxygen consumption for one bird (no. 2) that were approximately 50% less than those consumed by the other two birds in those treatments (Table 1.2). Mass-specific metabolic rates for the same bird flying out of ground effect were also much lower than other sampled birds. For flight in ground effect, this bird exhibited both stroke plane and tail angles substantially lower than those of the other two birds as well, which suggest that specific postural and kinematic changes may potentially increase savings for in ground effect hovering. However, a much increased sample size would be necessary to test this hypothesis.

Whereas Anna's hummingbirds tend to avoid flowers close to the ground in order to avoid terrestrial predators (Lima, 1991), observations of other hummingbird taxa suggest occasional flight near surfaces. For example, little hermits (Phaethornis longuemareus) forage for spider and insect prey in close proximity to the ground, and red-footed plumeleteers (Chalybura urochrysia) take arthropods from the upper surfaces of leaves (Stiles, 1995). We have also seen hovering hummingbirds picking insects directly off a dirt road in the Yucatan Peninsula (V.M.O.J. 2002, personal observation). Although it is unknown whether hummingbirds purposefully exploit the ground effect when either foraging for arthropods or during other activities, flight near vegetational surfaces at varied orientations is commonplace during nectar feeding by other taxa. Energetic advantages of flight near boundaries may thus yield a small, but significant reduction in overall foraging costs for many other species that fly near solid boundaries, including such insects as empidid flies, caddisflies, stoneflies, mayflies and some species of butterflies (e.g. species within the Cithaerias, Haetera and Pierella genera) (Dudley,

2000).

In conclusion, we found that hummingbirds obtain substantial mechanical and metabolic energy savings (of up to 24% and 34%, respectively) when hovering in ground effect compared with control conditions. Such savings result largely from the substantial decreases in the induced velocity; however, the region of upwash beneath the bird's body for in ground effect hovering most likely augments these reductions. Because vegetational boundaries, either horizontal or otherwise, characterize many flowers visited by volant nectar-feeding insects as well as vertebrates, these energetic effects are likely to be general and suggest the need for further studies of wake – ground and wake – body interactions in ground effect hovering.

bird #1		bird #2		bird #4	
mid-downstroke ($m\ s^{-1}$)	whole wingbeat ($m\ s^{-1}$)	mid-downstroke ($m\ s^{-1}$)	whole wingbeat ($m\ s^{-1}$)	mid-downstroke ($m\ s^{-1}$)	whole wingbeat ($m\ s^{-1}$)
3.48	3.18	3.65	3.21	4.21	3.31
3.93	3.28	4.12	3.42	4.22	3.18
3.77	3.18	4.01	3.1	3.98	3.22
4.74	3.9	3.68	3.67	3.87	3.87
4.46	3.68	4.33	3.6	4.12	3.69
4.21	3.75	3.89	3.57	5.08	3.57
3.95	3.39	4.01	3.41	3.98	3.51
3.71	3.6	4.00	3.35	4.21	3.71
4.19	3.72	4.19	3.54	4.17	3.65
4.19	3.53	4.17	3.45	4.32	3.45
4.41	3.77	4.33	3.67	4.67	3.51
4.43	3.62	4.42	3.88	4.28	3.65
3.84	2.97	3.97	3.01	4.01	3.21
4.75	3.94	4.01	3.48	4.01	3.47
4.18	3.61	3.98	2.78	4.09	3.11
4.77	3.9	4.01	3.88	3.89	3.28
4.33	3.89	4.56	3.36	4.21	3.76
4.00	3.74	4.21	3.91	4.36	3.76
4.21	3.86	4.32	3.79	4.19	3.88
4.32	3.65	4.07	3.87	4.09	3.61
4.21	3.74	3.87	3.99	4.22	3.76
4.24	3.88	4.44	3.98	3.89	3.67
4.23	3.22	4.24	3.26	4.54	3.19
5.19	4.05	4.74	3.99	4.87	3.89
4.32	3.23	4.54	3.46	4.88	3.78

Table 1.1. Mean wake velocity at mid-downstroke and for an entire wingbeat for three hummingbirds hovering at the control height (n=25 measurements per bird).

bird	treatment	χ (º)	γ (º)	β_h (º)	n (Hz)	Φ (º)	P_{met} (ml O_2 g^{-1} hr^{-1})	P_{mech} (W/N)	η (%)
#1	4 cm	19.7	-15.3	14.8	45.2	113.7	29.6	2.2	14.2
#2	4 cm	20.6	-34.3	10.1	49.5	107.5	18.7	2.2	22.3
#4	4 cm	21.7	11.6	20.4	43.6	114.9	33.8	2.1	11.5
#1	5 cm	23.7	1.5	11.9	44.7	112.9	34.8	2.3	12.7
#2	5 cm	21.7	-29.2	9.3	49.6	107.6	18.2	2.5	25.6
#4	5 cm	25.8	17.3	16.0	43.2	108.1	38.9	2.2	10.5
#1	6 cm	22.4	0.4	13.7	46.2	110.9	37.9	2.5	12.5
#2	6 cm	23.2	-15.8	9.9	50.7	105.9	18.8	2.6	26.0
#4	6 cm	27.0	28.1	20.5	41.6	115.3	42.0	2.4	10.9
#1	9 cm	34.8	30.4	15.3	44.2	118.7	47.2	2.6	10.6
#2	9 cm	34.9	26.2	10.6	49.4	105.9	39.4	2.8	13.2
#4	9 cm	31.1	41.6	21.2	42.2	121.1	44.8	2.7	11.6
#1	12 cm	40.8	42.7	13.2	43.0	121.6	47.1	2.7	11.0
#2	12 cm	31.1	21.9	12.2	50.4	107.0	36.6	2.9	15.3
#4	12 cm	32.9	39.7	14.9	42.3	116.8	51.2	2.80	10.4
#1	control	33.5	28.5	13.6	48.0	107.7	43.3	2.7	11.9
#2	control	35.7	33.2	11.2	47.9	113.4	36.0	2.9	15.4
#4	control	32.4	-44.1	16.8	44.0	117.3	45.3	2.9	12.0

Table 1.2. Mean values of wing and body kinematics, metabolic and mechanical power, and efficiency for three birds hovering at different treatment heights from the ground.

CHAPTER 2

VERTICAL ASCENDING FLIGHT OF ANNA'S HUMMINGBIRDS

Introduction

Little is known about the vertical flight abilities of animals, and sustained flight in either upward or downward directions remains relatively unexplored. Slow ascending flight in pigeons was characterized by Berg and Biewener (2008), but maximal performance is also of ecological relevance given its role in predator-prey interactions and any potential biomechanical limits impinging on escape. For hummingbirds in particular, vertical ascent can also play an important role in both mating and competitive displays. For example, males of *Selasphorus platycercus* and *Selasphorus rufus* perform rapid vertical climbs in order to gain a height advantage for attack maneuvers toward conspecific males (Clark et al., 2011) (Figure 2.1), while male and female *Mellisuga minima* ascend vertically as a pair, tens of meters high as a part of the courtship display (Clark, 2006). Many other hummingbird species similarly perform steep vertical climbs during competitive or courtship displays (see Clark, 2009; Wolf, 1976; Feinsinger, 1997; Stiles, 1982). While the kinematics and power requirements of male *Calypte anna* performing downward display dives have been analyzed in detail (Clark, 2009), its climbing flight has not yet been characterized, thus contributing to the motivating reasons behind the current study.

Whereas hovering flight has sometimes been described as the most energetically demanding mode of locomotion (e.g., Weis-Fogh, 1972), axial ascent must be even more challenging due to the supplemental costs entailed in increasing potential energy. Hummingbirds are known to hover under energetically challenging conditions, as occurs in hypo-dense air (Chai and Dudley, 1995; Chai and Dudley, 1996; Altshuler and Dudley, 2003) or with added loads imposed either artificially with external weights (Chai et al., 1997; Altshuler and Dudley, 2003) or naturally in the course of pre-migratory lipid loading (Wells, 1993). Given substantial power reserves relative to the needs of hovering, hummingbirds should be able to perform high-speed climbs up to speeds where mechanical power output becomes limiting.

In particular, we can estimate a hummingbird's maximum climb speed by using reported figures of excess power ΔP, i.e. the power available to a hummingbird in excess of that required for hovering. By ignoring the additional drag on the wings and the body incurred by a non-zero climb speed, and using the relations between climb speed, induced velocity, and thrust from momentum theory, the following equation can be derived (Johnson, 1980):

$$V = \frac{\Delta P}{T}\,\frac{2v_h+\Delta P/T}{v_h+\Delta P/T}, \tag{2.1}$$

where V is the climb speed, v_h is the induced velocity in normal hovering (which can be easily estimated), and T is the bird's vertical thrust, generally equivalent to its weight. Knowledge of ΔP thus enables a first-order estimate of climb speed, with maximum ΔP

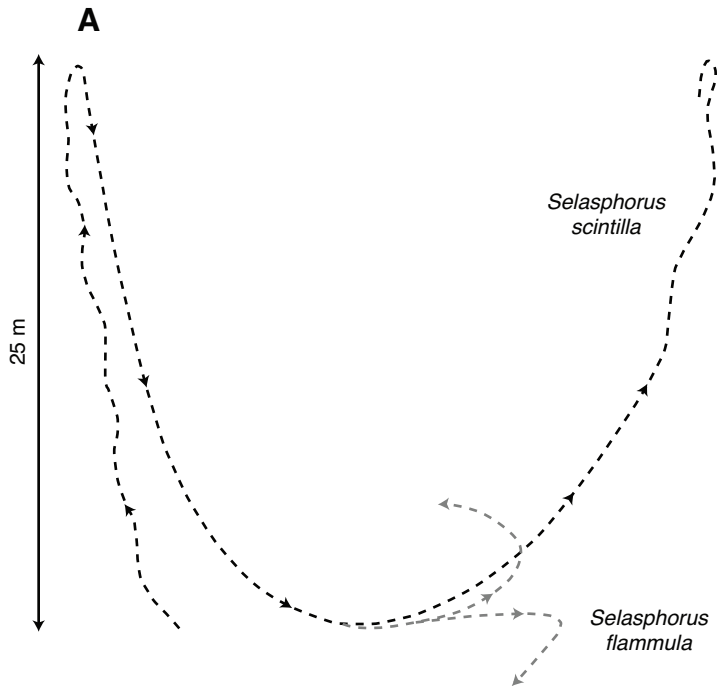

Figure 2.1. Dive schematics of *Selasphorus scintilla* and *S. flammula* (reprinted with permission from C. Clark [Clark et al., 2011]).

corresponding to maximum climb speed V_{max}. For ruby-throated hummingbirds (*Archilochus colubris*) performing transient hovering flight with maximum loads averaging 80% of body mass (Chai et al., 1997), application of Equation 2.1 yields a maximum climb speed of 3.9 m s^{-1}, based on the reported values of maximum mechanical power output, hovering mechanical power output, thrust, and induced velocity in that study. However, the upper limit to non-transient climbing may be somewhat lower than this value, due to the additional drag on the body and wings sustained during climbing flight. Whereas hovering with loaded weights or in low air density environments requires birds to generate sufficient power to stay aloft and meet induced power requirements, fast forward flight (i.e. horizontal flight) requires birds to generate sufficient power to overcome drag on the body and on the wings. Fast climbing flight, by contrast, combines all of these challenges, and thus may more generally indicate the limits to flight performance.

We therefore conducted an experiment in which Anna's hummingbirds (*Calypte anna*) flew within a vertical wind tunnel operated at variable speeds. When the bird maintains a stationary global position within a downward wind, vertical flight at high speed can be elicited. This approach is used to assess the vertical flight performance of rotors and helicopters, and was also employed in an early study of budgerigars flying at shallow ascent and descent angles (Tucker, 1968). Our first objective in this study was to delineate the limits to sustained axial climbing in hummingbirds. The second objective was to assess kinematic responses and mechanical power requirements under such extreme conditions, and to compare them with other flight modes for which maximal flight capacity has been previously assessed. Intriguingly, Berg and Biewener (2008) observed that the sum of level flight costs and the power necessary to increase potential energy did not differ from the total power required in climbing at any angle, for the domesticated pigeon *Columbia livia*. In contrast, the opposite was suggested in a study of pectoralis muscle performance in mallard ducks (*Anas platyrhynchos*) performing both level and ascending flight (Williamson et al., 2001). Thus, our third objective was to similarly answer whether the power required for axially climbing flight is equal to the sum of hovering power (i.e. P_{total} at V=0 m s^{-1}) and the increase in potential energy at equivalent vertical speed.

Materials and methods

Experimental Setup and Procedures

Four adult male Anna's hummingbirds (*Calypte anna*) were captured under permits from the California Department of Fish and Game and the U.S. Fish and Wildlife Service. Each bird was photographed with its right wing fully extended on a graph paper background to derive wing morphological parameters (in particular winglength R) using the *wingimageProcessor* program in Matlab (T. Hedrick; thedrick@bio.unc.edu). Body mass m was measured at both the start and end of experimental trials taken in a single day; the average of the two measurements was used in subsequent calculations. Following Chai and Dudley (1995), we assumed total wing mass and flight muscle mass to be 3% and 25% of body mass, respectively.

Our experimental setup consisted of a vertical wind fan (0.6 m diameter, Aerolab LLC, Laurel, MD, USA) modified with plexiglas walls and mesh fabric covering both the bottom surface and top opening to create an enclosed working section (Figure 2.2). Fan calibration and flow characterization were performed with a hot-wire anemometer (TSI Incorporated, Shoreview, MN, USA). Areas of spatially constant flow were mapped out, with these areas making up an annular shaped region centered on the middle of the working section, while the center and edges of the working section had more spatially and temporally varying flows. A perch and a 5 ml syringe filled with 20% Nektar-Plus solution (NEKTON GmbH, Pforzheim, Germany) attached to an artificial flower tip were positioned on opposite sides of the working section, within the aforementioned annular region and approximately 25 cm above the working section floor. Although the syringe was approximately 1.5 wingspans distant from the plexiglas wall, no wall effects on the flow could be detected at this distance.

Prior to experiments, birds were habituated within the working section for up to three hours on the preceding day. For each experimental trial, an individual hummingbird was placed into the tunnel's working section and allowed free access to the feeding syringe. Following an initial feeding bout, the syringe was removed from the working section; after 10–15 minutes, the syringe was returned and the fan was either left off (for hovering trials) or turned on at downward speeds of V=1, 2, 3, and 4 m s^{-1}, in a randomly selected order. This approach motivated the birds to hover-feed at the syringe for an extended period of time. Once having fed, birds were allowed free access to the syringe in still air for another 10–15 minutes. One feeding bout was analyzed per bird per downward wind speed. All four birds were tested at wind speeds ≤3 m s^{-1}; however, only two of the four birds were tested in the most extreme condition of V=4 m s^{-1}, due to this speed treatment being added halfway in the course of this study.

Video films for kinematic measurements were made using two high-speed cameras (AOS Technologies AG, Baden Daettwil, Switzerland), with one camera oriented vertically downwards above the syringe and the other camera oriented laterally within the plane of the syringe. Videos were recorded at 500 frames s^{-1} and subsequently analyzed in ImageJ (U.S. National Institutes of Health, Bethesda, MD, USA). For each recording, a segment of thirty to forty consecutive wingbeats was extracted from the middle of a feeding bout in which the bird's head remained stationary. For each of these wingbeats, the bird's horizontally projected stroke amplitude Φ_{hor}, wingbeat frequency n, mean angular velocity ω (calculated as twice the product of stroke amplitude and wingbeat frequency), body angle χ and tail angle γ (see Figure 1.1b) were measured.

Aerodynamic analysis

Under the assumption of perfect elastic energy storage (Greenewalt, 1960; Wells, 1993), the total mechanical power P_{total} for forward flight can be estimated by totaling the power required to overcome drag on the wings (profile power, P_{pro}), the power to overcome body drag (parasitic power, P_{par}), and the power to generate lift (induced power, P_{ind}) (Ellington, 1984*a-f*). We extended the estimate of P_{total} to climbing flight by first modifying P_{pro}, P_{par}, and P_{ind} to reflect the birds' non-zero vertical velocity

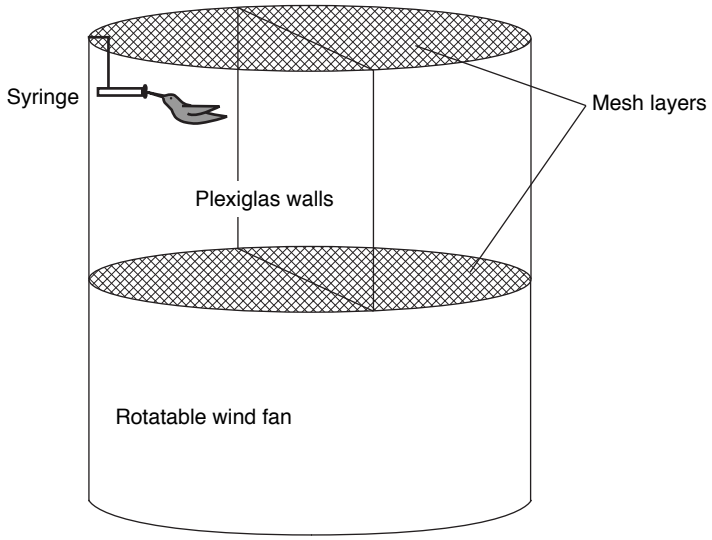

Figure 2.2. Vertical wind tunnel experimental setup.

component, and then including the power involved in changing potential energy (potential energy power, P_{PE}).

Profile power: We estimated P_{pro} with a quasi-steady model of profile drag (see Ellington, 1984*a-f*), using a drag coefficient of 0.139 (Altshuler et. al., 2004*b*) and assuming simple harmonic motion in order to approximate the time-derivatives of the positional angle of the wing within the stroke plane. The effect of the downward wind was directly incorporated into the calculation of P_{pro} by modifying the relative flapping velocity (U_r in equation 26 in Ellington [1984*f*]) to be the vector sum of the induced velocity, the flapping velocity, and the effective climbing velocity.

Parasite power: In hovering flight, the drag resulting from the interaction between the body and the downward momentum jet is generally considered to be negligible, and here we followed this assumption. By contrast, in forward horizontal flight, the parasite drag on the body, D_{par}, *i*ncreases in proportion to the square of flight speed, so that P_{par} increasingly dominates total flight power at higher speeds. Similarly, D_{par} must be a non-trivial force in fast climbing flight, and indeed will augment the bird's weight, mg. Assessing the parasite drag is difficult without detailed knowledge of the near field airflow around the body, so we used two indirect methods. In the first method, the maximum combined area of the head and body, A_{front}, as projected onto the horizontal plane, was measured from video recordings for each experimental subject at each downward speed condition. Using an empirically derived formula for the parasite drag coefficient, $C_{d,par}$, of diving passerine birds ($C_{d,par}=0.70–(5.8\times10^{-6})Re_b$, where Re_b is the Reynolds number of the body), we calculated the parasite drag force as $D_{par}=0.5\rho C_{d,par}A_{front}V^2$ (Hedenstrom and Liechti, 2001).

Our second method consisted of directly measuring the aerodynamic forces on a physical hummingbird model, whose posture as well as orientation relative to the wind stream could be manipulated (see Pennycuick, 1968 for similar procedure). We designed in Blender (the Blender Foundation, Amsterdam, Netherlands) and printed in Ponoko (Oakland, California) a three-dimensional wingless model with an adjustable neck and tail, based on dorsal and lateral images of one experimental subject engaged in ascending flight at V=0, 1, 2, 3, and 4 m s^{-1} (model construction methods closely followed Evangelista et al., 2014). We mounted the model onto a six-axis force sensor (Nano17, ATI, Apex, North Carolina) within the working section of the wind tunnel at the point where birds fed from the syringe. We then matched the model's posture and orientation with images taken from experimental videos, and measured subsequent drag forces under different wind speeds. These results were then scaled up or down for the other hummingbirds used in our experiments, based on $m^{2/3}$. As both methods have caveats, we chose to report any results dependent upon estimates of D_{par} separately, and used the subscript "*d1*" or "*d2*" to denote which drag method was used. Because parasite drag was assumed to be parallel to weight during climbing flight, these forces were summed into a single term (as in Wakeling and Ellington, 1997) and denoted as the thrust T (i.e. $T=mg+D_{par}$). As the velocity induced by the bird to generate enough lift to hover or move vertically depends upon the thrust (based on momentum theory for hovering flight; see Johnson, 1980; Ellington, 1984*a-f*), parasite power was therefore indirectly accounted for

within the estimates of P_{ind} and P_{pro} and thus not included as a separate individual term within the total power calculation.

Induced power: Downward momentum must be imparted to the air in order to maintain an upward, weight-offsetting force. For hovering flight, in which the velocity of the near wake is simply the induced velocity (Figure 2.3a), the hovering induced velocity v_h calculated from momentum theory is:

$$v_h = \sqrt{T/(2\rho A)}, \tag{2.2}$$

where $A=\Phi_{hor}R^2$ is the area of the idealized actuator disk, ρ is the air density, and k=1.2 is the correction factor accounting for tip losses and non-uniform inflow (Johnson, 1980; Ellington, 1984*e*).

In the case of axial climbing flight, the induced velocity decreases because of the addition of the climb velocity augmenting downward airflow through the actuator disc (Figure 2.3b). Momentum theory thus yields the following result:

$$v = -0.5V + \sqrt{(0.5V)^2 + v_h^2}, \tag{2.3}$$

where the induced velocity is now denoted simply as v, and is a function of both the hovering induced velocity v_h and the climb velocity V (Johnson, 1980; Azuma et al., 1985). In both hovering and climbing flight, the wake beneath the actuator disc advects away from the bird, with both the near and far wakes moving downward.

Total flow through the actuator disk is thus the sum of the induced velocity and the climb velocity ($v+V$), so that the combined induced and climb power is simply the product of the thrust and the total flow velocity. Here we separate this into induced power ($P_{ind}=Tv$) and potential energy power ($P_{PE}=TV$) (sometimes referred to as the climb power [MacAyeal et al., 2011]) for the sake of clarity. Therefore, total mechanical power output was estimated as:

$$P_{total}=P_{pro}+P_{ind}+P_{PE}. \tag{2.4}$$

Statistical Analysis

Effects of wind speed on kinematic variables and power estimates were tested using repeated measures ANOVA (rANOVA), with wind velocity modeled as the within-subject source of variation. Kinematic measurements were missing for the highest wind speed tested (4 m s^{-1}); this treatment was therefore excluded from statistical analyses. For each individual bird, values for kinematic variables and power estimates were normally distributed (based on the Shapiro-Wilk test for normality), and rANOVA was performed on mean values from each bird at each wind speed. A total of 16 flight sequences (4 birds × 4 speeds; V=0 to 3 m s^{-1} range) were statistically analyzed, with each sequence consisting of 30 – 40 wingbeats. Potential sphericity violations were tested with Mauchly's test; in cases in which the significance level α of the test was $\alpha<0.05$, the

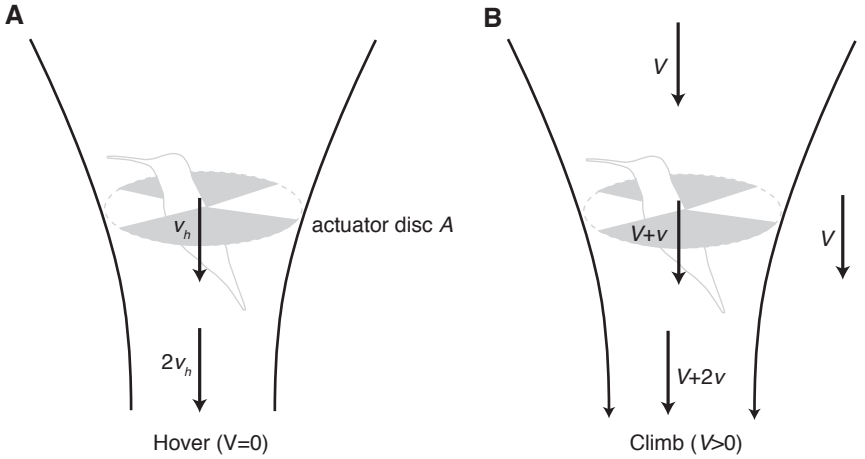

Figure 2.3. Momentum theory models for (A) hovering and (B) axial climbing flight. Shaded regions denote the area A of the actuator disc (where $A = \Phi_{hor}R^2$) (Adapted from Figure 4.3, Johnson, 2013).

number of degrees of freedom were modified using a conservative Greenhouse-Geisser correction. All statistical analyses were performed in R (R Foundation for Statistical Computing, Vienna, Austria), using the *ez* package (Lawrence, 2013).

Results

Hummingbirds (N=4: average mass m=4.8 g; average winglength R=51.9 mm) could sustain flight for more than 30 seconds in downward winds of 1, 2, and 3 m s^{-1}; by contrast, hovering within a downward wind of 4 m s^{-1} appeared to be much more challenging. While they could feed at this speed for durations of up to 10 s (i.e. >400 wingbeats), birds then immediately either perched or descended downward to the floor of the working section. Example wingtip trajectories of one subject engaged in climbing flight at 4 m s^{-1} (Figure 2.4A,B) and in hovering flight (Figure 2.4C,D) are shown from both the dorsal and lateral perspectives. At a downward speed of 5 m s^{-1}, no bird could sustain hover-feeding.

Repeated measures ANOVA indicated significant differences in much of the kinematic variables with downward wind speed over the range of 0 – 3 m s^{-1} (Table 2.1; Table 2.2). Thrust increased significantly from T=47 mN in hovering to T_{d1}=49 mN and T_{d2}=55 mN at V=3 m s^{-1} (p<0.001 for both values), and T_{d1}=53 mN and T_{d2}=61 mN at V=4 m s^{-1} (Figure 2.5A). As climb speed increased, both Φ_{hor} and n increased significantly, as well (Figure 2.5B). Stroke amplitude increased by an average of 12%, from 124±12˚ (mean ± 1 s.d.) in hovering to 139±2˚ at V=3 m s^{-1} (p=0.016), but increased by less than 1% from V=3 m s^{-1} to V=4 m s^{-1}. By contrast, n significantly increased from 43±3 Hz at hovering to 46±2 Hz at 3 m s^{-1} (p=0.006), or by 7%, and then increased by an additional 11% from 3 m s^{-1} to 4 m s^{-1}, such that wingbeat frequency reached 51±0 Hz at the maximum climb speed. Mean angular velocity also increased significantly with climb speed (p<0.001), from ω =184±7 rad s^{-1} at hovering to ω =224±7 rad s^{-1} at V=3 m s^{-1} (Figure 2.5C). Both the body and tail visibly became more vertically oriented as climb speed increased, as well (Figure 2.3B,D), although only changes in the tail angle were significant, with γ increasing from 57±11˚ at hovering to 74±9˚ at V=3 m s^{-1} (p=0.009) (Figure 2.5D).

All power estimates varied significantly with effective climb speed (0 to 3 m s^{-1} range) (p<0.001 for P_{ind}, P_{PE}, P_{pro}, and P_{total}) (Table 2.1; Table 2.2), regardless of which drag method was used. At low climb speeds, P_{ind} represented the majority of mechanical power expenditure, while P_{PE} and P_{pro} became progressively larger as climb speed increased (Figure 2.6A,B). Whereas induced power decreased by nearly one-half when V increased from 0 to 4 m s^{-1}, substantial increases in both profile power and potential energy power resulted in nearly two- and three-fold increases in total muscle mass-specific power, from P_{total}=114 W kg^{-1} in hovering to $P_{total,d1}$=223 W kg^{-1} and $P_{total,d2}$=247 W kg^{-1} at V=3 m s^{-1} (p<0.001, Table 2.2), and $P_{total,d1}$=293 W kg^{-1} and $P_{total,d2}$=341 W kg^{-1} at V=4 m s^{-1}, respectively.

Additionally, at 1 and 2 m s^{-1}, P_{total} significantly differed from P_{hov}+P_{PE}, regardless of which drag method was used, with the sum overestimating the actual total power at all

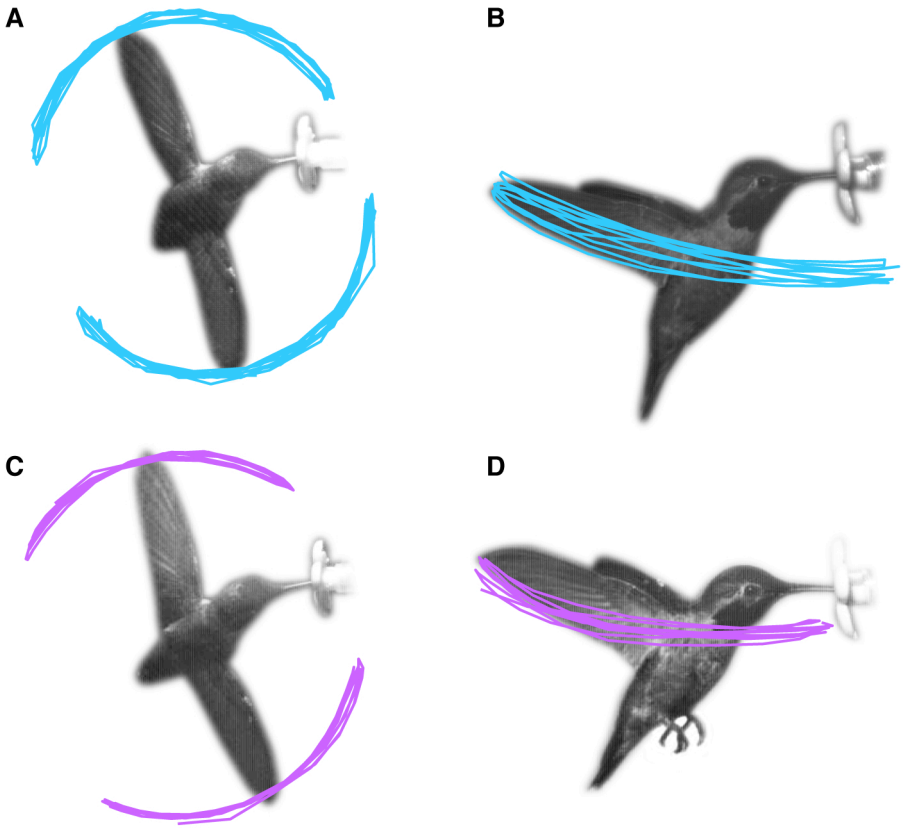

Figure 2.4. Example (A) dorsal and (B) lateral projections of wing trajectories over 0.1 s duration (~5.1 wingbeats), at V=4 m s^{-1}; example (C) dorsal and (B) lateral projections of wing trajectories, over 0.1 s duration (~4.3 wingbeats), at V=0 m s^{-1}. Bird is at mid-downstroke in dorsal images, and at supination (i.e. upstroke-to-downstroke transition) in lateral images.

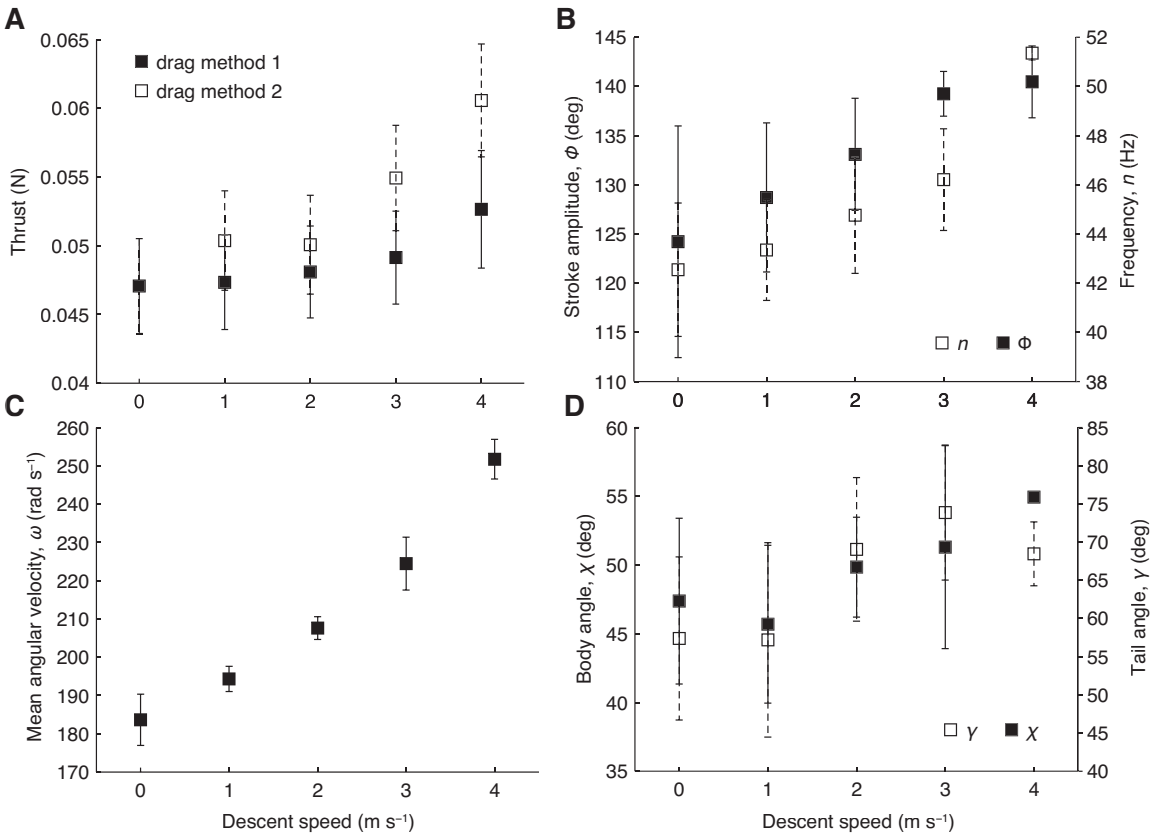

Figure 2.5. (A) Thrust *T,* based on the two different calculations of the drag force (where the first method used an empirically derived relation between body Reynolds number and parasite drag coefficient (Hedenstrom and Liechti, 2001), while the second method measured drag forces on a three-dimensional hummingbird model in a wind tunnel), (B) horizontal stroke amplitude Φ_{hor} and wingbeat frequency n, (C) mean wing angular velocity ω, and (D) body angle χ and tail angle γ, as a function of ascent speed. Data are given as mean ± 1 s.d., with N=4 at all speeds except V=4 m s^{-1}, where N=2.

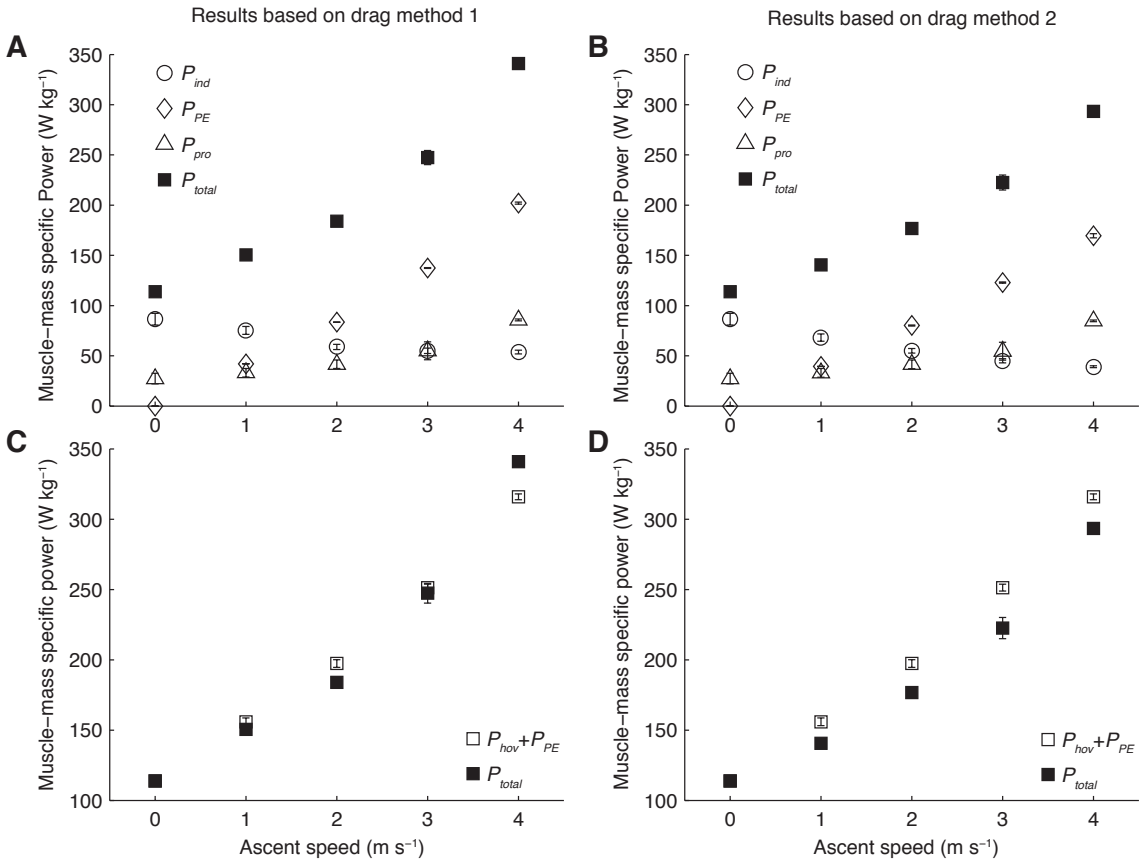

Figure 2.6. Muscle-mass specific powers (P_{ind}, P_{pro}, P_{PE}, and P_{total}) based on (A) drag method 1 and (B) drag method 2. Comparison of P_{total} with the sum of P_{PE} and P_{hov} (P_{hov}=P_{total} at V=0 m s^{-1} speed), based on (C) drag method 1 and (D) drag method 2. In the first set of comparisons (C), paired t-test results are as follow: p=0.0031 at V=1 m s^{-1}, p=0.0046 at V=2 m s^{-1}, and p=0.3363 at V=3 m s^{-1}. In the second set of comparisons (D), paired t-test results are as follow: p<0.001 at V=1 m s^{-1}, p=0.0034 at V=2 m s^{-1}, and p=0.0300 at V=3 m s^{-1}. Paired t-tests were not performed at V=4 m s-1, due to the sample size being too small at that speed for the test to have meaningful results.

Variable	0 m s^{-1}	1 m s^{-1}		2 m s^{-1}		3 m s^{-1}		4 m s^{-1}	
Φ (deg.)	124±12	129±8		133±6		139±2		140±4	
n (Hz)	43±3	43±2		45±2		46±2		51±0	
ω (rad s^{-1})	184±7	194±3		208±3		224±7		252±5	
χ (deg.)	47±6	46±6		50±4		51±7		55±0	
γ (deg.)	57±11	57±13		69±9		74±9		68±4	
T (mN)	47±3	47±3	50±4	48±3	50±4	49±3	55±4	53±4	61±0
P_{ind} (W kg^{-1})	87±6	68±4	75±4	55±2	59±3	45±2	55±3	39±1	54±2
P_{PE} (W kg^{-1})	0±0	39±0	42±0	80±1	83±0	123±1	137±0	169±2	202±1
P_{pro} (W kg^{-1})	27±5	33±4	33±4	41±4	42±4	55±9	55±9	85±1	86±1
P_{total} (W kg^{-1})	114±3	141±2	150±2	177±4	184±3	223±7	247±7	293±0	341±1
$P_{hov}+P_{PE}$ (W kg^{-1})	114±3	153±3	156±3	194±3	197±3	237±2	251±2	285±0	316±2

Values are mean ± 1 s.d. (N=4, except at V=4 m s^{-1}, where N=2).

Variables: Φ, stroke amplitude; n, wingbeat frequency; ω, mean angular velocity; χ, body angle; γ, tail angle; T, thrust; P_{ind}, muscle mass-specific induced power; P_{PE}, muscle mass-specific potential energy power; P_{pro}, muscle mass-specific profile power; P_{total}, muscle mass-specific total power; and $P_{hov}+P_{PE}$, sum of muscle mass-specific total power to hover (i.e. P_{total} at V=0 m s^{-1}) and P_{PE}. For variables which have two results reported, the first and second sets of results are based on the first and second different methods of drag estimation, respectively.

Table 2.1. Summary of flight performance of Anna's hummingbirds (*Calypte anna*) at climbing flight speeds of 0, 1, 2, 3, and 4 m s^{-1}.

Variable	*F-value*		*P-value*	
Φ	5.982		0.016	
n	8.358		0.006	
ω	38.238		<0.001	
χ	1.1386		0.3847	
γ	12.8201		0.009*	
T	204.980	1703.805	<0.001	<0.001*
P_{ind}	292.886	234.306	<0.001	<0.001
P_{PE}	93126.9	323979.9	<0.001*	<0.001*
P_{pro}	50.780	52.099	<0.001	<0.001
P_{total}	678.513	1180.054	<0.001	<0.001*

*Did not meet sphericity requirement (Mauchley's test for sphericity yielded $p<0.05$). Number of degrees of freedom were modified with Greenhouse-Geisser corrections.

Table 2.2. Statistical results from repeated measures ANOVA testing the effect of climbing flight at 0-3 m s^{-1} speeds (N=4; d.f. 3, 9).

of the speeds tested (Figure 2.6C,D; Table 2.1). However, based on drag method 1, these two values were not significantly different at V=3 m s^{-1} (p=0.3363), while based on drag method 2, the two values were just significant (p=0.0300) (Figure 2.6C,D). The difference at V=-4 m s^{-1} was not tested, as the sample size was too small for the paired t-test to have meaningful results.

Discussion

Maximum ascent speed for the hummingbirds studied here was about 4 m s^{-1}, which is much higher than the transient climbing flight speeds reported for other volant taxa (e.g., 2.6 m s^{-1} for the domestic pigeons *Columba livia* [Dial and Biewener, 1993] and 0.5 m s^{-1} for the bat *Cynopterus brachyotis* [MacAyeal et. al, 2011]). Hummingbirds also differed here in that such extreme flight performance could be sustained for several hundreds of wingbeats. Normalized maximum climbing speed is equally impressive. For example, a "*very high* climb rate [emphasis added]" for helicopters is considered to be at a speed of V/v_h=1 (Johnson, p. 115, 1980). By contrast, maximum vertical ascents obtained here represent an almost doubling of this value, with maximum average V/v_h equal to 1.80. Interestingly, the 4 m s^{-1} maximum sustained climb speed identified here is very close to the initially hypothesized speed of 3.9 m s^{-1}, despite the large difference between the actual total maximum power results ($P_{total,d1}$=293 W kg^{-1} and $P_{total,d2}$=341 W kg^{-1}) and the estimated total maximum power that was used in Equation 2.1 (206 W kg^{-1} for *A. colubris* hummingbirds hovering with maximal loading [Chai et al., 1997]). Because the additional power required to overcome profile and parasitic drag forces, which was neglected in our estimate of V_{max} in Equation 2.1, happened to be almost equal to the disagreement between the actual and estimated maximum total mechanical powers, such a coincidence resulted.

One of our objectives in this study was to assess whether the power required to axially climb is equal to the sum of hovering power (i.e. P_{total} at V=0 m s^{-1}) and the increase in potential energy at equivalent vertical speed. For hummingbirds engaged in axial ascending flight, the answer is no. Our results most likely differed from those of Berg and Biewener (2008) because we tested relatively fast flight at the maximum 90° climb angle (i.e. axial flight with no horizontal velocity component at all), whereas Berg and Biewener looked at comparatively shallow climbing flight in which the pigeons were primarily flying forwards. Thus, changes in the sum of the induced velocity, parasite drag, and profile drag in our study – all parameters which P_{hov} and P_{PE} neglect – are nontrivial (Figure 2.6A,B; Table 2.1; Table 2.2), in contrast to the aforementioned study

Animal flight performance can be limited by a variety of factors, including mechanical strength of the wings, physiological constraints of the respiratory and cardiovascular systems, and power output of the flight muscle (Alexander, 2004; Hughes and Rayner, 1991). The extremely high mechanical power output at the highest climb speed tested in this study suggests that the limiting factor to climb speed is sufficient mechanical power generation of the muscles. Estimates of maximum total mechanical power ($P_{total,d1}$=293 W kg^{-1} and $P_{total,d2}$=341 W kg^{-1}) match well with theoretical maximum values of vertebrate muscle (290-325 W kg^{-1}), assuming the particular

mitochondrial density and sinusoidal contraction velocity of hummingbird muscle (Wells, 1993; Pennycuick and Rezende, 1984). These values are also similar to the 309 W kg^{-1} maximum burst power output of *Lampornis clemenciae* and *Eugenes fulgens*, two hummingbird species that are almost double the mass of *C. anna* at 8.4 g and 7.4 g, respectively (Chai and Millard, 1997). However, these values are much higher than the maximum burst power outputs estimated for the slightly smaller hummingbird species *Archilochus colubris* (*m*=3.0 g), *Archilochus alexanderi* (*m*=3.0 g), and *Selasphorus rufus* (*m*=3.3 g) hovering with maximum loading, where P_{total}=206 W kg^{-1}, 228 W kg^{-1}, and 88 W kg^{-1}, respectively (Chai et. al, 1997; Chai and Millard, 1997).

In the abovementioned maximum load-lifting studies, the duration of maximum load lifting was counterbalanced with the mass of the load, such that larger species could lift proportionally more, but for shorter durations, than smaller species. In contrast, *C. anna* engaged in vertical climbing flight in this study are able to both generate as well as maintain a very high mechanical power output. Whereas our estimates of P_{PE} are robust, values of P_{pro}, P_{ind}, and the implicit P_{par} involve a number of assumptions. Previous studies, for example, assumed a slightly lower profile drag coefficient than used here; additionally, parasite drag force in this study could have been overestimated, which would increase all of the power estimates at maximum climb. However, for a hummingbird climbing at V=4 m s^{-1}, the mechanical power required to change potential energy alone is already 185 W kg^{-1}, which is more than double the maximum burst power output for *S. rufus* hovering with maximum loading. Furthermore, the large rise in wingbeat frequency when climbing must substantially increase total power as well, regardless of the specific profile drag coefficient used. While we assumed that the wings moved with perfect elastic storage based on previous studies (e.g. Wells, 1993), such an assumption may not necessarily hold true (Van den Berg and Rayner, 1995); inclusion of inertial costs would markedly increase total mechanical power as well. Taking all of this into account, the extremely high value of total maximum mechanical power is therefore not altogether surprising; rather, it is more interesting to examine the particular changes in wing kinematics that occurred as climb speed increased.

Both wingbeat frequency and stroke amplitude increased from n=43 Hz and Φ=124° at hovering to n=51 Hz and Φ=140° at the maximum climb speed, for an overall 19% increase in frequency and 13% increase in stroke amplitude. For the wings to work optimally, flapping frequency should be fixed at a specific resonant frequency of the flight apparatus (Chai and Dudley, 1998; Greenewalt, 1975), and thus modulation of stroke amplitude should theoretically be favored over modulation of wingbeat frequency. Stroke amplitude modulation has indeed been shown to be the primary means for controlling force power output within and among hummingbird species (Chai and Dudley, 1998; Chai and Dudley, 1995; Chai and Millard, 1997; Chai et al., 1997), with frequency generally increasing only when stroke amplitude has already reached its maximum 180° limit (e.g. Altshuler and Dudley, 2003).

Thus, kinematic differences between this study and aforementioned hummingbird studies eliciting maximum performance may reflect varying behavioral contexts of extreme flight. For example, bats performing vertical takeoff and climbing flight

controlled mechanical power output by increasing wingbeat frequency while decreasing stroke amplitude, in contrast to other flight modes (MacAyeal et al., 2010). One study of pigeons (*C. livia*) in ascending flight found that increases in power output are met primarily by increases in pectoralis muscle strain via larger wing stroke amplitudes, with smaller increases in muscle force production and wingbeat frequency (Dial and Biewener, 1993). Conversely, another study on pigeons performing climbing flight at various angles found no significant changes in either kinematic variable relative to horizontal flight (although flight angle and flight speed were not independently controlled in that study, and thus kinematic changes due to vertical climbing flight may have been obscured) (Berg and Biewener, 2008).

Alternatively, the kinematic results of this experiment may differ from previous studies on maximum hummingbird flight performance because of biomechanical species-specific differences. Specifically, hummingbird taxa are not equal in their ability to effectively modulate stroke amplitude (Altshuler and Dudley, 2003). As stroke amplitude cannot exceed 180° due to adverse interference and even physical contact between the wings (Chai and Dudley, 1995), hovering flight with a high stroke amplitude is limited in reserve capacity, i.e. the percentage increase possible in Φ. *C. anna*, however, as a lowland species, has a comparatively small hovering amplitude of 124±12˚ (Table 2.2; see also Kim et al., 2014; Sapir et al., 2012). If wingbeat frequency were invariant while stroke amplitude increased from 124˚ to 180˚, *C. anna* would theoretically be able to generate just enough mechanical power for 4 m s^{-1} vertical climbing flight, but would do so at a seemingly impossibly high stroke amplitude increase of ~45%. This is more than double that of many other hummingbird species' stroke amplitude reserves, which are around 19% (Altshuler and Dudley, 2003; Chai and Dudley, 1998). Here, stroke amplitude increases only to about 140º (Figure 2.5B), and it is uncertain if *C. anna* can increase this value further. These results suggest that the specific biomechanical design of *C. anna* may constrain them in such a way that a combination of increasing both stroke amplitude and flapping frequency is necessary, particularly for vertical flight.

In observations of male Anna's hummingbirds performing both aggressive and courtship displays, Stiles (1982) estimated that climb speeds were "*only* around 4-5 m s^{-1} [emphasis added]". Contrary to his perception, our results thus indicate that these birds were ascending at *maximum* velocities in their displays. Furthermore, birds repeatedly perform these displays up to ten times in rapid progression (Stiles, 1982). It is known that in addition to morphological and physiological traits, biomechanical and physiological capacities can reflect underlying selective forces (Chai and Dudley, 1998). The sophisticated displays of male *C. anna*, for example, suggest selection for high speed diving capability, with speeds approaching 27.3 m s^{-1} (Clark, 2009). It would be of interest to examine whether other hummingbird species that engage in similar displays also exhibit the kinematic and energetic capacities elicited here from *C. anna*. In particular, if the downward components of display dives correlate with male fitness (Clark, 2009), it is possible that speed of ascent is under comparable selection.

CHAPTER 3

VERTICAL DESCENDING FLIGHT OF ANNA'S HUMMINGBIRDS

Introduction

One may consider vertical flight as simply flying with steady gains or losses in gravitational potential energy, such that the mechanisms to ascend or descend only involve increasing or decreasing lift via changes in angle of attack, wing area, amplitude, wing-stroke pattern, or other kinematic variables (Alexander, 2004). While an animal's climb speed is constrained by how much mechanical power the muscles can generate (as shown in Chapter 2), it has been proposed that an animal's descent speed is limited by how much body drag can be reduced, such that maximum descent speed is equal to an animal's terminal velocity (Alexander, 2004). However, in contrast to gliding, falling, and diving, this simplistic framework does not take into account the issues of control and stability that an animal may face in the course of *steady* (i.e. non-accelerating) descending flight. Examples of this flight mode can be observed in nectarivorous insects and hummingbirds during foraging trips, or in any volant animal maintaining its position within a thermal or updraft. An especially captivating instance of controlled vertical descending flight can be seen in the flocks of swifts (e.g. *Chaetura pelagica* or *Chaetura vauxi*) flying downwards into their roosts within various vertical, hollow manmade structures, such as chimneys, airshafts, cisterns, and wells (Price, 2014; Thompson, 1977). In all of these descents, in either the absolute or relative sense with respect to the surrounding air, position control and thus precise force modulation is paramount.

An animal manipulates the air around itself, generating downwards momentum, in order to stay aloft and fly. Generally, the interaction between an animal and its wake is negligible; when an animal hovers or flies forward, wingtip vortices are periodically shed, advecting away and eventually dissipating due to friction. In some instances, however, the wake continues to have an effect on the animal. In the case of hovering near ground surfaces, for instance, the interaction between an animal, its shed vortices, and the ground surface causes both mechanical power output and metabolic power input to dramatically decrease as a function of ground proximity (Chapter 1; Kim et al., 2014). The effect of an animal's wake on its energetics and kinematics may be even greater in the case of vertically descending flight. In this situation, an animal must still generate downwards momentum; however, because the animal is also flying downwards, it will fly directly into its own downwash. In the case of slow-to-moderate axial descending in manmade vertical takeoff and landing aircraft (VTOL), such as helicopters, the vortices shed by the rotors do not advect away but instead accumulate and become trapped beneath the rotor plane, forming a ring vortex flow pattern (Stack et. al. 2005, Green et. al. 2005). Such a situation is aptly termed 'vortex ring state (VRS)' (alternatively, 'turbulent wake state') and manifests itself by strong recirculation and unsteady, turbulent flow (Johnson, 1980; Leishman, 2006). Aircraft caught in VRS experience adverse conditions, such as vibrations, substantial fluctuations in rotor thrust, and increased induced power requirements, resulting in compromised flight performance and safety. Thus, there is much renewed interest in better understanding descending axial flight, and

in particular, VRS.

While animals are arguably much more sophisticated flyers than manmade rotorcraft, vertical descending flight may yet present the same set of challenges, namely VRS. Whether animals must overcome the same aerodynamic challenges, or alter their kinematics in such a way to avoid such situations, is not well known. There has been relatively little research on the vertical descending flight of animals (Berg and Biewener, 2008), and particularly on the kinematic correlates of such flight mode (Dudley, 2002). Thus, in this study we sought to characterize the steady vertical descending flight of Anna's hummingbirds (*Calypte anna*) by obtaining wing kinematics, measurements of metabolic energy, and estimates of mechanical power output with respect to axial descent speed. We predict that hummingbirds will be proficient in their vertical descending flight capabilities, as earlier studies have demonstrated their capacity to fly under a variety of challenging conditions, such as hovering under loads of up to 80% body mass (Chai et al., 1997) or flying forward in relatively turbulent von Kármán vortex streets (Ortega-Jimenez et al., 2014), and thus illustrate their kinematic and energetic reserves. We hypothesize that both mechanical and metabolic power will decrease with speed, while muscle efficiency will remain invariant. Furthermore, we expect that issues of stability and control will be the primary challenges to descending flight, with these manifesting through greater wingbeat frequency as well as increased variance in kinematic variables.

Materials and Methods

Experimental Setup and Procedures

Our experimental setup was identical to that in Chapter 2. Four adult, male Anna's hummingbirds (the same individuals as in Chapter 2) were used for both kinematic and metabolic experiments. For each trial, an individual hummingbird was placed into the experimental volume (Figure 2.1) with still air, and allowed to feed. Following the initial feeding, the syringe was removed; after ten minutes, the fan was either left off (for 0 m s^{-1} trials) or turned on, and the syringe was placed back into the volume. This procedure encouraged birds to feed for an extended period of time while still ensuring respiratory quotients near 1 (Welch, 2011; Suarez et al., 1996). Once the bird fed, the fan was turned off, if it was on, and the bird was allowed free access to the syringe in still air for another ten minutes. For metabolic measurements, this procedure was then repeated, with randomly ordered wind velocities. For kinematic measurements, one feeding bout was analyzed per bird per wind velocity, with the wind speed order also randomly selected. The vertical wind speeds tested in this experiment ranged from 0-4 m s^{-1}, with 1 m s^{-1} increments. However, while all four birds were tested in wind speeds $\leq$3 m s^{-1}, only two of the four birds were tested in the most extreme wind speed of 4 m s^{-1}.

Kinematic measurements were made via two high-speed cameras (AOS Technologies AG, Baden Daettwil, Switzerland) positioned above and lateral to the wind tunnel setup, and subsequently analyzed in ImageJ (U.S. National Institutes of Health, Bethesda, MD, USA). For each recording, a segment of thirty to forty individual wingbeats was taken from the middle of the feeding duration in which the bird's head

maintained a stationary position. For each wingbeat, the bird's horizontally projected stroke amplitude Φ_{hor}, flapping period n^{-1}, mean wing angular velocity ω, body angle χ (see Figure 1.1b) and tail angle γ (see Figure 1.1b) were measured. Body mass m was measured at both the start and end of a run of trials taken in a single day; the mean body mass was then used for any further analyses involving measurements from that particular day. Wing mass was estimated as 3% body mass, while muscle mass was estimated as 25% body mass (Chai and Dudley, 1995).

The metabolic power input P_{input} was estimated from measurements of total oxygen consumption and feeding bout duration, which were taken via an oxygen analyzer (Foxbox, Sable Systems Inc., Las Vegas, NV, USA) connected to a mask equipped with an LED and photo-resistor (Bartholomew and Lighton, 1986) (metabolic measurement setup was identical to Kim et al., 2014; Chapter 1). Expirated air was drawn into the mask at a rate of 1200 ml s^{-1} and then dried with Drierite (Xenia, OH, USA) before passing into the oxygen analyzer. As oxygen values rarely reached steady state, we used the formula:

$$\dot{V}_{O_2} = \frac{FR\left(F_iO_2 - F_eO_2\right)}{\Delta t} \tag{3.1}$$

in order to estimate the instantaneous oxygen consumption rate $\dot{V}_{O_2}$ (Bartholomew and Lighton, 1986; Welch, 2011). In equation 3.1, FR is the flow rate through the system, F_iO_2 and F_eO_2 are the fractional O_2 concentrations in the incurrent and excurrent airstreams respectively, and Δt is the total time the bird's head was inside the mask, which was obtained from the voltage readings in the photo-resistor circuit (Bartholomew and Lighton, 1986) (Δt is different from total bout duration, as birds generally went into and out of the mask several times within a single feeding bout). 10-15 measurements per wind velocity were taken for each bird, with all measurements made from feeding bouts with durations greater than 2 s (Welch, 2011).

Aerodynamic analysis

As in Chapter 2, the mechanical power requirements for hovering and descending flight were estimated using a combination of momentum theory, extended to vertical flight (Johnson, 1980), and Ellington's aerodynamic model for hovering animal flight (1984*a-f*). The sign convention that positive thrust points upward while positive wind velocity points downward is utilized, so that hovering flight and descending flight are denoted in the rest of this paper by $V=0$ and $V<0$ respectively, where V refers to the wind velocity vector (Johnson, 1980) (Figure 2.3; Figure 3.1).

The mechanical power required for forward flight is usually calculated by individually estimating the components that make up the total power. In the case of perfect elastic storage, for instance, the total mechanical power P_{total} consists of the power required to overcome drag on the wings (profile power, P_{pro}), the power to overcome parasitic (body) drag (P_{par}), and the power to offset body weight (induced power, P_{ind}). In order to estimate the total mechanical power required for descending flight, we modified the individual power components to reflect the non-zero vertical

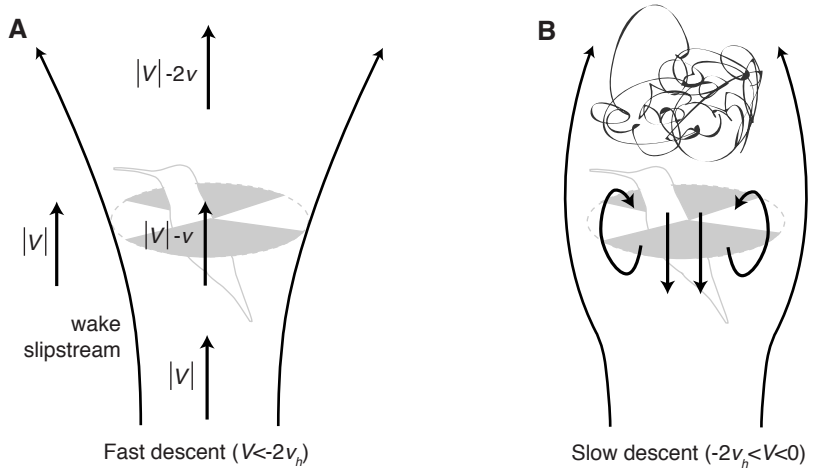

Figure 3.1. Momentum theory models for (A) fast descending and (B) slow descending flight. Shaded regions denote the area A of the actuator disc (where $A = \Phi_{hor} R^2$) (Adapted from Fig. 4.3, Johnson, 2013).

velocity component. Profile power was estimated by using a quasi-steady model of profile drag, with the vertical wind added into the vector sum of the relative wingtip velocity vector (equation 26, Ellington, 1984*f*). Parasitic drag and power were estimated as in Chapter 2, with the assumption that parasitic drag was anti-parallel to weight (such that the drag effectively added an upward, buoyant force on the bird). Thus, we again combined the weight and drag forces into a single term denoted as the thrust T (similar to Wakeling and Ellington, 1997). Again, as in Chapter 2, because we used two different methods to estimate parasitic drag force, any subsequent results dependent upon D_{par} are given separately, with the subscript "*d1*" or "*d2*" to denote which method of drag estimation was used. Because the thrust was modified to reflect the parasitic drag on the bird, parasitic power was implicitly calculated within any term that depended upon T, and therefore not included as a separate term within the calculation of P_{total}.

Induced power: By Newton's law, downward momentum must be imparted to the air in order to maintain an upward, weight-offsetting force. Momentum theory, which is based upon the conservation laws of mass, momentum, and energy, enables us to estimate the speed of the air accelerated by the flapping wings through the idealized actuator disc. For hovering flight, in which the velocity of the wake is simply the induced velocity (Figure 2.3A), the hovering induced velocity v_h is calculated from Equation 2.2. In the case of climbing flight (V>0), however, the induced velocity decreases due to the addition of the climb velocity augmenting the downward airflow in the actuator disc (Figure 2.3B), such that momentum theory results in Equation 2.3 (the induced velocity for climbing flight). In both hovering and climbing flight, the wake of the actuator disc advects away, with both the near and far wakes moving downward. The flows through the disc and inside the slipstream are downward, while the air outside of the slipstream is either still (during hover) (Figure 2.3A) or descending downward as well (during climb) (Figure 2.3B). In both of these situations, the flow field can be modeled with some degree of accuracy, and thus the induced velocity and power can be reasonably estimated (Johnson, 1980).

In the case of descending flight (V<0), however, air is not moving downward everywhere, as the climb model assumes. Indeed, when V<0, two regimes exist: one in which the descent speed is great enough such that the flow is moving upward everywhere and therefore analytically solvable:

$$v = -0.5V - \sqrt{(0.5V)^2 - v_h^2} \tag{3.2}$$

(Figure 3.1A), and another in which the descent speed is not so great for this to be the case, i.e. VRS (Johnson, 1980). In the latter situation, the flow field is considerably more complicated, characterized by recirculation and turbulence (Figure 3.1B). Both the climb solution (Equation 2.3) and the fast descent solution (Equation 3.2) cannot be used when the descent speed is in the range of $-2v_h<V<0$, as both result in a physically impossible but numerically correct situation in which the flow is downward in the far wake but upward everywhere else. In this flight regime, there is neither a well-defined slipstream nor a well-defined wake, and therefore no suitable simple model for calculating the induced velocity.

Despite this, the climb equation (Equation 2.3) was used for calculating the induced velocity in descending flight. A version of this equation, modified to reflect the non-axial descent angle, was also used for calculating the induced velocity in a study of pigeons (*C. livia*) performing both ascending and descending flights (Berg and Biewener, 2008). Although the flow model is incorrect, the momentum theory climb solution is valid to some extent in descending flight; experimental data on helicopters and rotors puts the extent to which the climb solution (i.e. momentum theory) is reasonably appropriate in VRS as down to V/v_h=-1.5 (Johnson, 2013). In our experiment, V=-4 m s^{-1} corresponds to an average normalized velocity of V/v_h=-1.36, V=-3 m s^{-1} corresponds to V/v_h=-1.29, V=-2 m s^{-1} corresponds to V/v_h=-0.91, and V=-1 m s^{-1} corresponds to V/v_h=-0.44. Nevertheless, the induced velocities that are estimated, as well as any subsequent figures that depend upon them, should be taken cautiously and considered to be minimum values at best.

The total induced power was then calculated as the product of the thrust and the total flow through the actuator disk, i.e. $T(v+V)$ (Wakeling and Ellington, 1997, Johnson, 1980). In some studies, the velocity components are separated into two terms and therefore give rise to two (nominally) separate powers: induced power ($P_{ind}=Tv$) and "potential energy power" ($P_{PE}=TV$) (Askew et. al, 2001; Berg and Biewener, 2008; MacAyeal et. al. 2011; Kim and Dudley, 2014). To combine or separate the terms is only a matter of notation; in this chapter, as in Chapter 2, we chose to separate the terms for the sake of clarity. Therefore, the total power output for descending flight was estimated as $P_{total}=P_{pro}+P_{ind}+P_{PE}$ (i.e. Equation 2.4).

Efficiency

We calculated a form of efficiency as the ratio of flight power output to flight power input, where flight power output is the aforementioned P_{total} and flight power input P_{input} is derived from $\dot{V}_{O_2}$. We used a respiratory quotient of one (Suarez et al., 1986) and a conversion factor of 21.1 J ml^{-1} O_2 (Brobeck and Dubois, 1980) in order to convert oxygen consumption rates into the appropriate units. As metabolic energy is used not only for flight muscles, but also for maintaining posture and other necessary functions not directly related to flight (Morris et. al. 2010), efficiency was calculated as:

$$\eta=P_{total}/(0.9P_{input}), \tag{3.3}$$

where we assumed that 10% of the metabolic power was used for posture maintenance.

Statistical Analysis

The statistical significance of wind velocity on kinematic, metabolic, and aerodynamic variables was tested using repeated measures analysis of variance (rANOVA), with wind velocity modeled as the within-subject source of variation. Kinematic and metabolic measurements at 4 m s^{-1} winds were missing for two birds; therefore, a balanced statistical design was achieved by restricting the rANOVA analysis

to the 0-3 m s^{-1} wind speed range. Analyses were performed on the mean values for each wind speed from each bird. Sphericity violations were tested with Mauchly's test; in cases in which the significance level α of the test was $\alpha<0.05$, the number of degrees of freedom (d.f.) was modified using a Greenhouse-Geisser correction. All analyses were performed in R (R Foundation for Statistical Computing, Vienna, Austria), using the *ez* package (Lawrence, 2013).

Results

Wing and body kinematics dramatically altered as descent speed increased. Examples of wing trajectories (over a duration of 0.1 s) as well as body posture at V=0 m s^{-1} (hovering) and at V=-4 m s^{-1} are shown in Figure 3.2. At V=0 m s^{-1}, no rolling or yawing of the body could be observed, with birds not deviating from their position while hover-feeding. Wing movement was highly symmetric (between the left and right wings) as well as highly repetitive from wingbeat to wingbeat, with wings sweeping primarily back and forth within a plane (e.g. Figure 3.2C; Figure 3.2D). In contrast, at V=-4 m s^{-1}, while the birds' heads did not move, their bodies exhibited a high degree of both rolling and yawing. There was much greater asymmetry between the wings, particularly in their instantaneous vertical positions and chord angles (i.e. pitch). A 'stroke plane' was not as easily definable, with wings moving back and forth as well as up and down (e.g. Figure 3.2A, Figure 3.2B). Additionally, the wings behaved less rigidly, resulting in much deformation of their structures (see videos for example). At speeds in-between hovering and V=-4 m s^{-1}, body and wing kinematics displayed characteristics intermediate to those at the minimum and maximum speeds tested.

More specifically, as descent velocity increased from hovering to V=-3 m s^{-1} and to V=-4 m s^{-1}, thrust decreased significantly from T=47 mN at hovering to T_{d1}=44 mN and T_{d2}=35 mN at V=-3 m s^{-1} ($p<0.001$), and T_{d1}=42 mN and T_{d1}=27 mN at V=-4 m s^{-1} (Table 3.1, Table 3.2; Figure 3.3A). Stroke amplitude also decreased from 124° in hovering to 94° at V=-3 m s^{-1} and 49° at V=-4 m s^{-1}, i.e. by 24% and 60%, respectively (Table 3.1; Figure 3.3B), where the difference in the 0 to -3 m s^{-1} range was found to be significant ($p<0.001$; Table 3.2). Frequency, in contrast, increased from n=43 Hz at V=0 m s^{-1} to n=47 Hz at V=-3 m s^{-1} and n=46 Hz at V=-4 m s^{-1} (Table 3.1; Figure 3.3B), with this difference being just significant (p=0.040) in the 0 to -3 m s^{-1} range (Table 3.2). Due to the interaction between stroke amplitude and flapping frequency, mean wing angular velocity decreased significantly with increasing descent speed, from 184 rad s^{-1} at hovering to 153 rad s^{-1} at V=-3 m s^{-1} ($p<0.001$) and 79 rad s^{-1} at V=-4 m s^{-1} (Figure 3.1C, Table 3.1, Table 3.2). Both body and tail angles also decreased significantly, such that the bird's posture became more horizontally oriented as descent speed increased (e.g. Figure 3.2B, Figure 3.2D; Figure 3.3D; Table 3.1; Table 3.2).

Induced power nearly doubled with increasing descent speed, regardless of which drag estimation method was used ($p<0.001$ for both) (Figure 3.4A,B; Table 3.1; Table 3.2); in contrast, both potential energy power and profile power decreased considerably ($p<0.001$ for both variables; Table 3.1; Table 3.2), resulting in an overall decrease in total mechanical power, from P_{total}=114 W kg^{-1} in hovering to $P_{total,d1}$=63 W kg^{-1} and

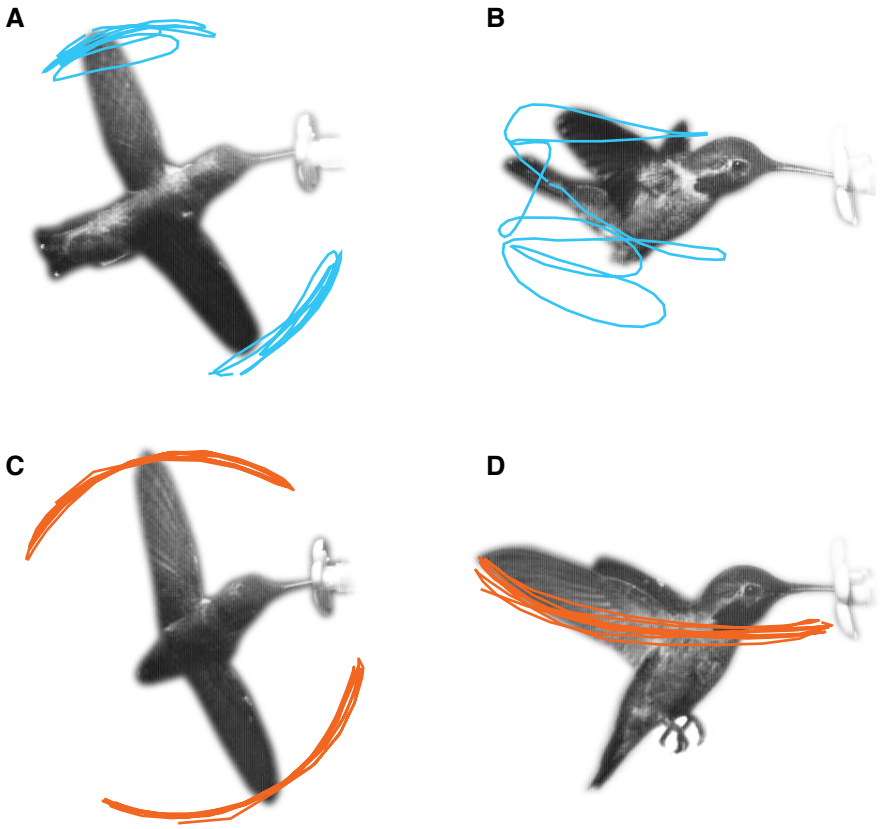

Figure 3.2. Example (A) dorsal and (B) lateral projections of wing trajectories over 0.1 s duration (~4.5 wingbeats), at V=-4 m s^{-1}; example (C) dorsal and (B) lateral projections of wing trajectories, over 0.1 s duration (~4.3 wingbeats), at V=0 m s^{-1}. Images and trajectories come from a single bird. Bird is at mid-downstroke in the wingbeat cycle in dorsal images, and at supination (i.e. upstroke-to-downstroke transition) in lateral images.

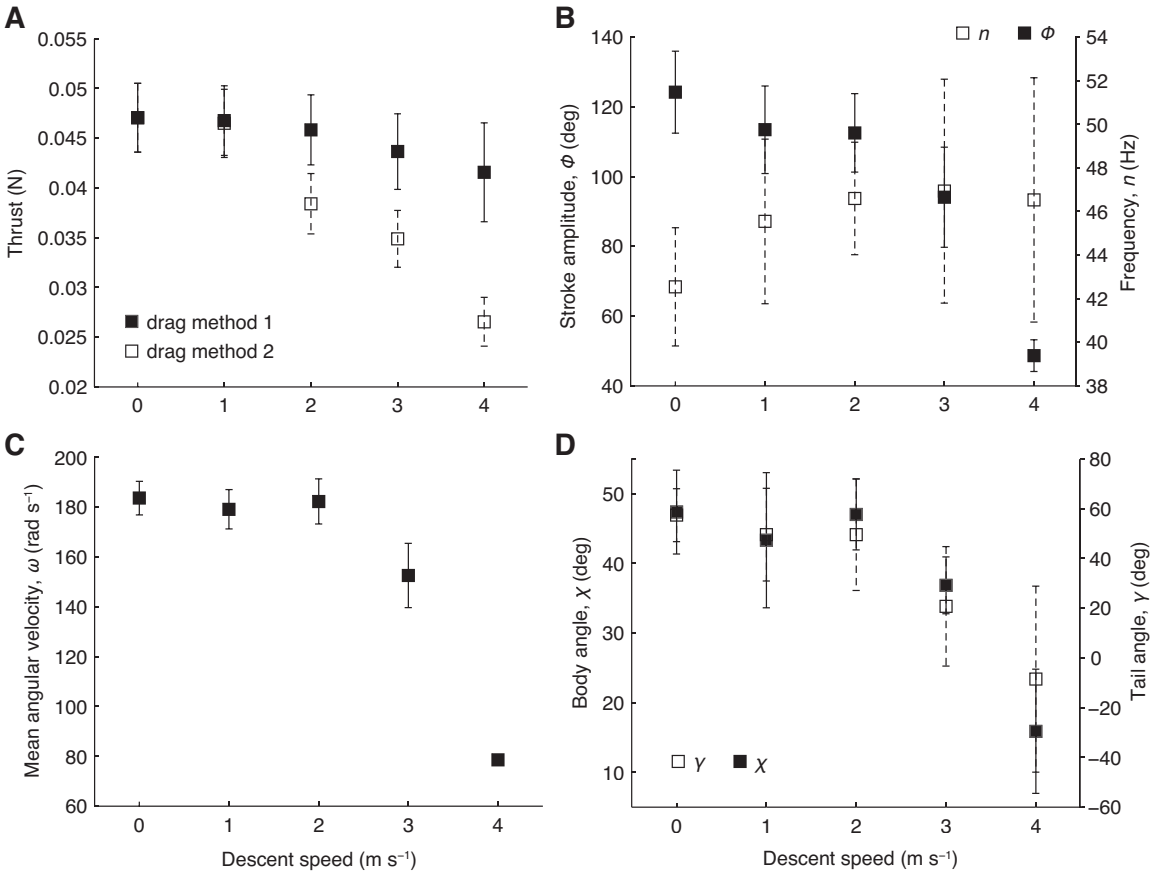

Figure 3.3. (A) Thrust *T,* based on the two different calculations of the drag force (where the first method used an empirically derived relation between body Reynolds number and parasite drag coefficient (Hedenstrom and Liechti, 2001), while the second method measured drag forces on a three-dimensional hummingbird model in a wind tunnel), (B) horizontal stroke amplitude Φ_{hor} and wingbeat frequency n, (C) mean wing angular velocity ω, and (D) body angle χ and tail angle γ, as a function of ascent speed. Data are given as mean±s.d., with N=4 at all speeds except V=4 m s^{-1}, where N=2.

Variable	0 m s^{-1}	1 m s^{-1}		2 m s^{-1}		3 m s^{-1}		4 m s^{-1}	
Φ_{hor} (deg.)	124±12	113±13		113±11		94±14		49±5	
n (Hz)	43±3	46±4		47±3		47±5		46±6	
ω (rad s^{-1})	184±7	180±8		182±9		153±13		79±2	
χ (deg.)	47±6	43±10		47±5		37±4		16±9	
γ (deg.)	57±11	50±19		50±22		21±24		-9±37	
T (mN)	47±4	47±4	47±3	46±4	38±0	44±4	35±0	42±5	27±0
P_{ind} (W kg^{-1})	87±6	111±4	110±4	134±5	106±4	159±4	121±3	193±6	118±3
P_{PE} (W kg^{-1})	0±0	-39±0	-39±1	-76±0	-87±1	-109±1	-87±1	-134±4	-88±2
P_{pro} (W kg^{-1})	27±5	25±4	25±4	26±6	26±6	15±5	15±5	3±0	2±0
P_{total} (W kg^{-1})	114±3	97±3	96±3	83±3	68±3	65±3	49±3	63±2	32±1
$P_{hov}+P_{PE}$ (W kg^{-1})	114±3	75±3	75±3	37±3	50±3	5±2	27±2	-18±2	25±2
$\dot{V}_{o_2}$ (ml O_2 kg^{-1} hr^{-1})	49±6	43±9		41±8		31±11		23±7	
η (%)	11±1	11±3	11±3	10±2	8±1	11±6	9±4	13±4	7±2

Values are mean±s.d. (N=4, except at V=-4 m s^{-1}, where N=2).
Φ, stroke amplitude; n, wingbeat frequency; ω, mean angular velocity; χ, body angle; γ, tail angle; T, thrust; P_{ind}, muscle mass-specific induced power; P_{PE}, muscle mass-specific potential energy power; P_{pro}, muscle mass-specific profile power; P_{total}, muscle mass-specific total power; $\dot{V}_{o_2}$, oxygen consumption (metabolic rate); η, muscle efficiency.

Table 3.1. Summary of flight performance of Anna's hummingbirds (Calypte anna) at descending flight speeds of 0, 1, 2, 3, and 4 m s^{-1}.

Variable	*F-value*		*P-value*	
Φ_{hor}	17.009		<0.001	
n	4.239		0.0399	
ω	17.997		<0.001	
χ	4.6223		0.032	
γ	7.1528		0.009	
T	306.870	1700.619	<0.001	<0.001*
P_{ind}	1105.383	190.239	<0.001	<0.001
P_{PE}	18605.04	47980.23	<0.001*	<0.001*
P_{pro}	24.230	24.856	<0.001	<0.001
P_{total}	742.809	1101.193	<0.001	<0.001
$\dot{V}_{o_2}$	32.564		<0.001	
η	0.5046	5.918	0.689	0.016

*Did not meet sphericity requirement (Mauchley's test for sphericity yielded $p<0.05$). Epsilon values were corrected with Greenhouse-Geisser corrections.

Table 3.2. Repeated measures-ANOVA results assessing variation over 0-3 m s^{-1} descending speed range (N=4; d.f. 3, 9).

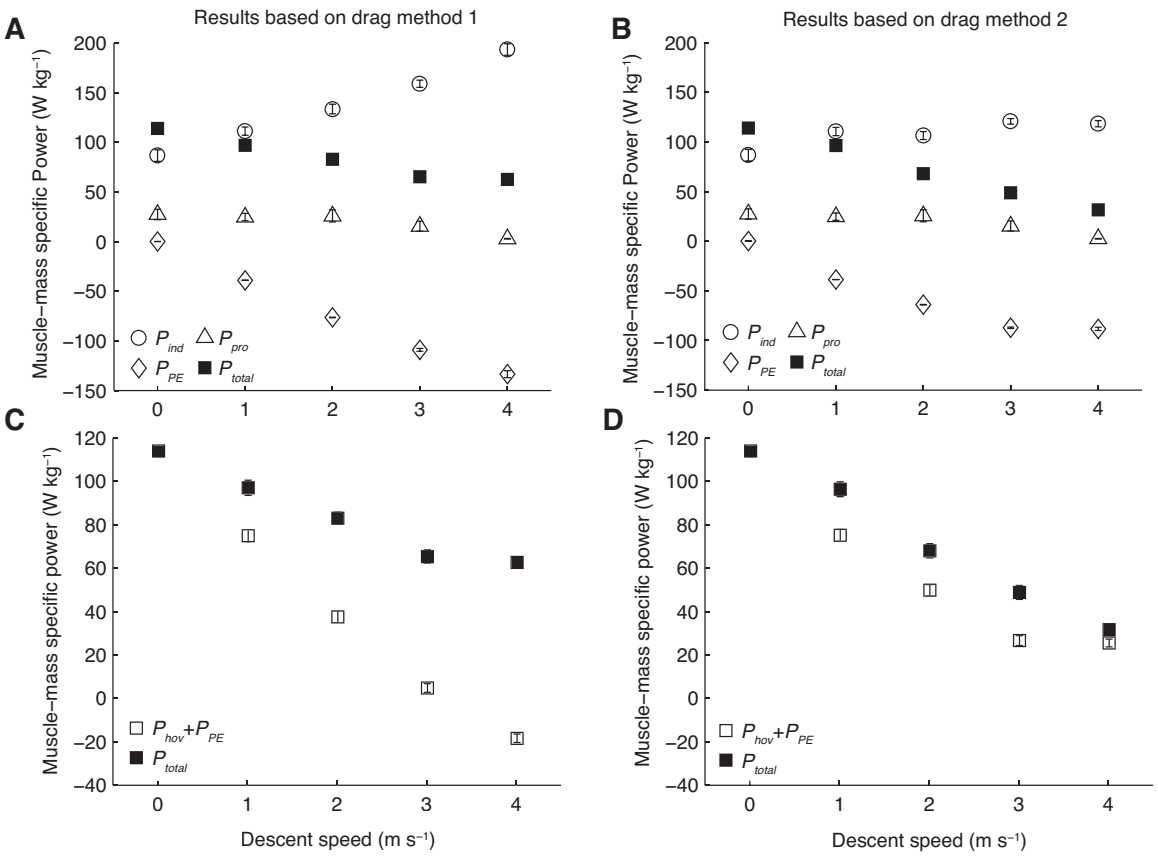

Figure 3.4. Muscle-mass specific powers (P_{ind}, P_{pro}, P_{PE}, and P_{total}) based on drag method 1 (A) and drag method 2 (B). Comparison of P_{total} with the sum of P_{PE} and P_{hov} (P_{hov}=P_{total} at V=0 m s^{-1} speed), based on drag method 1 (C) and drag method 2 (D). In both sets of comparisons, p<0.001 for V=1, 2, and 3 m s^{-1}. Paired t-tests were not performed at V=4 m s-1, due to the sample size being too small at that speed for the test to have meaningful results.

$P_{total,d2}$=32 W kg^{-1} in V=-3 m s^{-1} (p<0.001) and 46 W kg^{-1} in V=-4 m s^{-1} (Table 3.1; Table 3.2; Figure 3.4A,B). Metabolic power also significantly decreased, from 49 ml O_2 g^{-1} hr^{-1} in hovering to 31 ml O_2 g^{-1} hr^{-1} in V=-3 m s^{-1} (p<0.001; Table 3.1; Table 3.2) and 23 ml O_2 g^{-1} hr^{-1}in V=-4 m s^{-1} (Figure 3.5A). Although both P_{per} and metabolic power decreased, the significance of descent speed on flight muscle efficiency depended upon which drag method was used. The first drag method resulted in a constant level of efficiency, with η ranging from 11 to 13% (p=0.689); the second drag method, however, resulted in muscle efficiency significantly decreasing with increasing descent speed (p=0.016) (Table 3.1, Table 3.2, Figure 3.5B). When comparing mechanical power at V=-1, -2, and -3 m s^{-1}, P_{total} significantly differed from P_{hov}+P_{PE} (p<0.001 at these speeds, regardless of which drag method was used) (Figure 3.4C,D) (the difference at V=-4 m s^{-1} was not tested, as the sample size was too small for the paired t-test to have meaningful results).

The standard deviations of the wing kinematic variables significantly increased with descent speed, as well. The mean of the individual birds' standard deviations of horizontal stroke amplitude increased from s.d.(Φ_{hor})=4.5° in hovering to s.d(Φ_{hor})=6.9° in V=-3 m s^{-1} (p=0.0207) and s.d(Φ_{hor})=11.1° in V=-4 m s^{-1} (Figure 3.6A; Table 3.3), while that of flapping frequency increased from s.d.(n)=1.3 Hz in hovering to s.d.(n)=2.3 Hz and s.d.(n)=2.4 Hz in V=-3 m s^{-1} (p=0.0078) and V=-4 m s^{-1}, respectively (Figure 3.6B, Table 3.3).

Discussion

All of the birds tested could sustain descending flight at all wind speeds, including the maximum velocity of V=-4 m s^{-1}. That the hummingbirds could perform a 90° controlled vertical descent at this speed is impressive, considering the unique challenges of descending flight, and flight into turbulent conditions in general. In a study of pigeons performing various flight modes, the maximum angle of descent that pigeons were capable of was 80° (Dial and Biewener, 1993). While the speed for this angle of descent is unreported, the vertical component of velocity for pigeons descending at 60° is -2.9 m s^{-1} (Berg and Biewener, 2008). In that study, descent speed decreased with increasing descent angle, which suggests that pigeons descending at greater angles presumably do so at speeds less than -2.9 m s^{-1}. However, it is not clear from our study if V=-4 m s^{-1} is the maximum speed of controlled, steady descent capable of hummingbirds.

In contrast to vertical climbing flight (Chapter 2), in which Anna's hummingbirds exhibited amongst the highest reported figures of mechanical power output for vertebrates, vertical descending flight resulted in extremely low values of both metabolic power and total mechanical power. The metabolic power at V=-4 m s^{-1} ($\dot{V}_{O_2}$=23±7 ml O_2 g^{-1} hr^{-1}) for instance, approached the reported resting metabolic rate of Anna's hummingbirds ($\dot{V}_{O_2}$=14 ml O_2 g^{-1} hr^{-1}; Pearson, 1950). Changes in the body and tail kinematics suggest that hummingbirds were augmenting parasitic drag by increasing their frontal area, in order to decrease the power requirements of staying aloft. While we did not measure the wings' chord angles (i.e. pitch), at mid-downstroke and mid-upstroke,

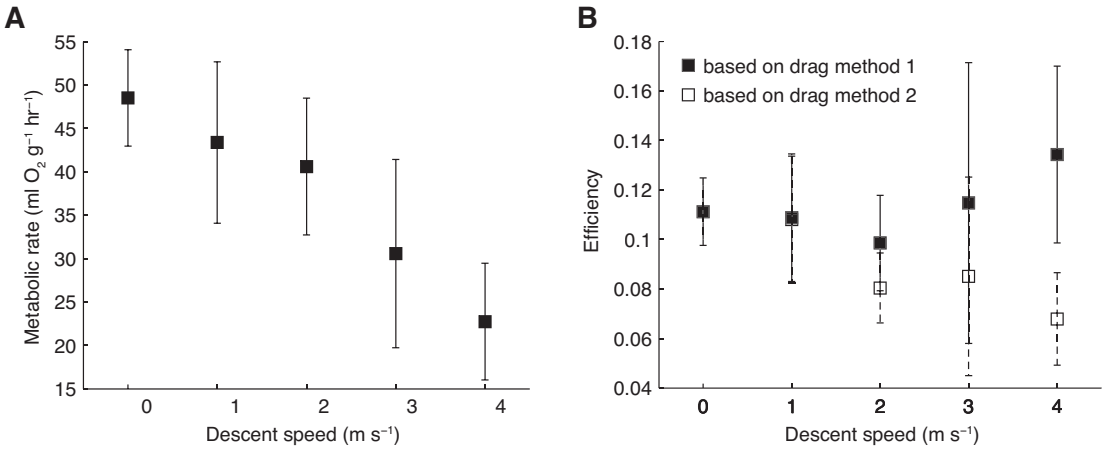

Figure 3.5. (A) Metabolic rate and (B) muscle efficiency, as a function of descent speed.

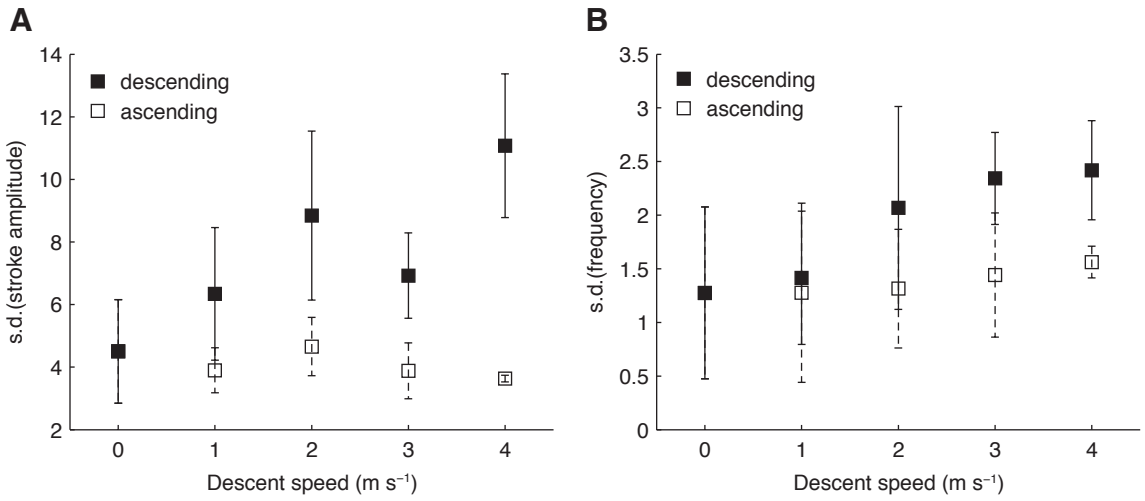

Figure 3.6. (A) Standard deviations of stroke amplitude (Φ_{hor}) and (B) flapping frequency (n) with respect to vertical speed. Values are means of individual birds' *standard deviations*. For both kinematic wingbeat variables, descending flight consistently had greater wingbeat to wingbeat variation than ascending flight. S.d.(Φ_{hor}) and s.d.(n) varied significantly across 0-3 m s^{-1} descent speeds (repeated-measures ANOVA: Φ_{hor}: p=0.0207, F=5.441; n: p=0.0078, F=7.571); in contrast, s.d.(Φ_{hor}) and s.d.(n) did not vary across 0-3 m s-1 ascent speeds (repeated-measures ANOVA: Φ_{hor}: p=0.6011, F=0.6526; n: p=0.6606, F=0.5501.

Variable	**0 m s^{-1}**	**1 m s^{-1}**	**2 m s^{-1}**	**3 m s^{-1}**	**4 m s^{-1}**
s.d.(Φ_{hor})	4.5±1.7	6.3±2.1	8.8±2.7	6.9±1.4	11.1±2.3
s.d.(n)	1.3±0.8	1.4±0.6	2.1±0.9	2.3±0.4	2.4±0.5

Table 3.3. Summary of variation in wing kinematic variables at descending flight speeds of 0, 1, 2, 3, and 4 m s^{-1}.

these angles were visibly shallower with respect to the horizon at V=-4 m s^{-1} than at lower descent speeds, such that a greater area of the wings was perpendicular to the flow, creating more upwards drag on the bird. Thus, while P_{ind} naturally increased with descent speed (due to the bird having to contribute more towards the downwards flow through the actuator disc), thrust, P_{pro}, and P_{PE} substantially decreased, causing the overall decreases in P_{total} with descent speed. However, while the first drag method resulted in no significant change in efficiency with increasing descent speed, with η ranging from 10% to 13%, the second drag method resulted in a significant decrease in efficiency with increasing descent speed, with η changing from 11% in hovering to 7% at V=-4 m s^{-1}. Previous studies reporting the muscle efficiency of hummingbirds give mixed results, with efficiency remaining invariant in ruby-throated hummingbirds hovering in heliox treatments (Chai and Dudley, 1995) as well as in Anna's hummingbirds hovering in ground effect (Kim et al., 2014; Chapter 1), but increasing significantly (from 10% to 11%) in ruby-throated hummingbirds hovering in helium treatments (Chai and Dudley, 1996). Whether these differences in muscle efficiency result from differing flight modes is not clear.

When we assessed whether the total power to fly at different vertical speeds was equivalent to the sum of the power to perform level flight (in this case, hovering flight) and the power to change potential energy, we found that these two values were different at every speed, with p<0.001 at all speeds tested regardless of which drag method was used. By contrast, for pigeons performing 30° and 60° ascending and descending flights, the differences between P_{total} and P_{hov}+P_{PE} were insignificant at all angles (Berg and Biewener, 2008). However, the difference was greatest for the steepest descent flight in the aforementioned study, due to the large induced power requirements. While every difference was significant in our study, the differences grew with increasing descent speed, reflecting the higher values of P_{ind} as well. Thus, while total power to ascend or descend may be estimated at shallow angles with the simple summation of the powers to perform level flight and change potential energy (Berg and Biewener, 2008), this estimate is clearly disastrous in flights with steeper angles at greater speeds, in which changes in the induced velocity are non-trivial; at descent speeds greater than 3 m s^{-1}, for instance, this approximation potentially underestimates total power by more than threefold (Figure 3.4C).

As descent speed increased, the wingbeat to wingbeat variation of the wing kinematics for each bird increased significantly, with s.d.(Φ_{hor}) increasing by 153% and 247% from hovering to V=-3 m s^{-1} and V=-4 m s^{-1}, respectively (p=0.0207) (Figure 3.6A), and s.d.(n) increasing by 177% and 185% from hovering to V=-3 m s^{-1} and V=-4 m s^{-1}, respectively (p=0.0078) (Figure 3.6B) (Table 3.3). In contrast, the standard deviations of both frequency and stroke amplitude for Anna's hummingbirds performing climbing flight remained invariant with respect to flight speed (p=0.6011 and p=0.6606 for variation in Φ_{hor} and n, respectively) (Chapter 2). Increases in wing kinematic variation and flapping frequency were also observed in Anna's hummingbirds flying in von Kármán vortex streets (Ortega-Jimenez et al., 2014); increases in the flapping frequency of pigeons performing near-vertical descending flight were reported as well (Dial and Biewener, 1993). These results suggest that although hummingbirds were able to sustain

descending flight with little power expenditure, issues of control and stability become less trivial as descent speed increases. As the airflow becomes progressively chaotic, the increased variation in wingbeat kinematics, as well as the overall increases in flapping frequency (Figure 3.3B), may allow the hummingbird to better modulate its aerodynamic force production and thus maintain its stable position at the feeder.

Unlike a helicopter, an animal can sense the flow around itself and dynamically adjust to it, and perhaps even prevent a disastrous situation like vortex ring state despite flying axially downward at speeds clearly within the turbulent regime. Interestingly, a previous study showed that the peak forces developed by the primary flight muscles (pectoralis) of rock pigeons (*Columba livia*) performing near-vertical descents are drastically larger than in steady, level flight, with values not significantly different than those in takeoffs and vertical ascents (Biewener and Dial, 1993). Additionally, the force profiles among consecutive wingbeats have more variation in near-vertical descending flight than in level, climbing, or taking-off flight modes (Biewener and Dial, 1993). These studies, along with our results, suggest that fine-tuning the wing kinematics to successfully perform descending flight requires additional power, though these increases are more than offset by the decreases in potential energy.

Estimations of induced, profile, and parasitic powers all relied upon several assumptions, and so the power results presented here should be taken as minimum values. Most seriously, induced power relied upon technically incorrect usage of momentum theory; modifications to this estimate would certainly drive P_{total} upwards. Particle image velocimetry measurements of the induced velocity, qualitative pictures of the wake (as in Figure 1.5A, for example), and more detailed wing and body kinematics (such as characterization of the wings' flexion) of an animal performing vertical descent would be particularly informative for better understanding how an animal performs flapping descending flight. Further studies investigating the kinematic changes required of hummingbirds and other flyers to adapt to chaotic and turbulent flow conditions, and the metabolic cost increases, if any (such as in hummingbirds performing fast flight in turbulent wakes [Ortega-Jimenez et al., 2014]), would be additionally interesting.

CHAPTER 4

FORWARD ASYMMETRIC FLIGHT KINEMATICS OF ANNA'S HUMMINGBIRDS

Introduction

Maneuverability generally refers to the ability of flying animals to alter the speed and orientation of their movements about the three translational and three rotational degrees of freedom, via the rapid production and modulation of forces by wings and other aerodynamically active structures (Dudley 2000, 2002). Similarly, the contrasting ability to respond to external perturbations for the maintenance of stable body posture or aerial trajectory in flight also depends on the efficacy of force and torque modulation (Taylor and Thomas, 2002; Tobalske, 2007). Fundamental to both maneuverability and stability is the ability of the wings on either side to produce disparate aerodynamic forces. During hovering or forward flight at uniform velocity, these forces and rotational torques are necessarily balanced via symmetric wing and body kinematics. In contrast, turning maneuvers, including body roll and yaw, derive from bilaterally asymmetric deployment of the two wings.

For many flying animals of different taxa, the ability to redirect aerodynamic forces with respect to the body-axis is constrained, requiring changes in body orientation, also known as force-vectoring, to redirect the aerodynamic forces in the direction required by any given aerial maneuver (Dudley, 2000; Fry et al., 2003; Hedrick et al., 2007; Warrick and Dial, 1998; Norberg, 1990; Iriarte-Diaz and Swartz, 2008). For instance, pigeons are unable to reorient resultant forces laterally to generate the centripetal force required to overcome inertia during low-speed turns without rolling their bodies into a banked angle (Warrick and Dial, 1998; Ros et al., 2011). Hummingbirds, by contrast, have shown the ability to redirect forces relative to their bodies during pure yaw turns by employing bilaterally asymmetric stroke amplitudes and deviations while maintaining constant body position angles (Altshuler et al., 2012).

Hummingbirds are unique among vertebrates in their extreme metabolic and flight capabilities. While the ability to perform hovering flight is a unique behavioral feature of hummingbirds among vertebrate taxa, they are also exceptionally maneuverable, capable of quick alterations in flight speed, body orientation, and flight trajectory relative to other birds (Altshuler and Dudley, 2002). Consistent across these various flight capabilities is the hummingbird's exceptional dominion over its aerodynamics. Hummingbirds have available to them several variables for altering the production of lift on each wing, such as modulating the relative incident air velocity over their wings, the lift coefficient (primarily via changes to the angle of attack), and the surface area of the wing (Warrick and Dial, 1998). Compared to the extensive body of work on hovering (e.g. Greenewalt, 1960; Weis-Fogh, 1972; Epting, 1980; Bartholomew and Lighton, 1986; Wells, 1993; Chai and Dudley, 1996; Altshuler and Dudley. 2002; Warrick et al., 2005; Tobalske et al., 2007), much less has been done to investigate forward flight at higher speeds, particularly in non-uniform and non-steady state conditions that are more representative

of the natural conditions hummingbirds must regularly negotiate and which will likely elicit bilaterally asymmetric responses.

Therefore, the purpose of this study was to infer which of these aerodynamic mechanisms hummingbirds, specifically the species *Calypte anna*, utilize to compensate against bilaterally disparate forcing while maintaining stable flight, as well as the degree to which they can decouple the production and orientation of aerodynamic forces between the two wings. Specifically, we compared the flight kinematics of hummingbirds immersed in a spatially uniform airflow with those of hummingbirds immersed in an asymmetric airflow, in which the airspeed of one side was approximately twice that of the other. We not only expect bilateral symmetry to be very strong in the uniform flow configuration, but we expect that the values of the kinematic variables for both wings will be predicted to some extent by measurements made by a study on the kinematics of *Selasphorus rufus* hummingbirds engaged in forward flight at various speeds (Tobalske et al., 2007). We expect the wingbeat kinematics measured in the asymmetric configuration to exhibit increased bilateral asymmetry compared to the control.

Materials and Methods

Experimental setup

Three male Anna's hummingbirds (body mass m=4.6 ± 0.4 g, left wing length R_l=5.1 ± 0.1 cm, right wing length R_r=4.9±0.2 cm, mean ± 1 s.d.) were trained to simultaneously fly and feed from a 0.5 ml syringe filled with 20% Nektar-Plus (Nekton, Pforzheim, Germany) solution within the working section of an Eiffel-style open-circuit wind tunnel (Model 404, Engineering Laboratory Design, Inc., Lake City, MN, USA). The working section, located downwind of a 6.25:1 contraction, measured 45.5 cm × 45.5 cm in the cross-section and 91.5 cm in length. Two distinct wind profile configurations were created by inserting different frames into a slot directly upstream of the working section: a uniform airspeed profile symmetric in both cross-stream axes and a sheared profile with airspeed asymmetry about the tunnel's lateral midline (Figure 4.1). We established the uniform profile by placing a screen-less frame into the slot, and used this as the control treatment. Conversely, we created an asymmetric airspeed profile by installing a framed metal grate with two layers of fine nylon mesh fastened over the left half of the grating. The nylon screens attenuated airflow through the left half of the working section, establishing a "plane mixing layer" with the free stream velocity on the right side greater than that of the left side, with a velocity inflection point centered about the lateral midline of the tunnel.

The airspeed within the working section was controlled by specifying the wind tunnel fan's rotational speed, which was set at a constant 38 Hz for both profile configurations in this study. To center the bird's position relative to the sheared profile's inflection point during flight, we positioned the syringe along the lateral midline of the working section, 6 cm behind the upwind boundary and 10 cm below the ceiling. The syringe was suspended from the roof of the working section by a 1 mm diameter steel wire, and oriented downstream at a 35° angle below the horizon to reduce flight

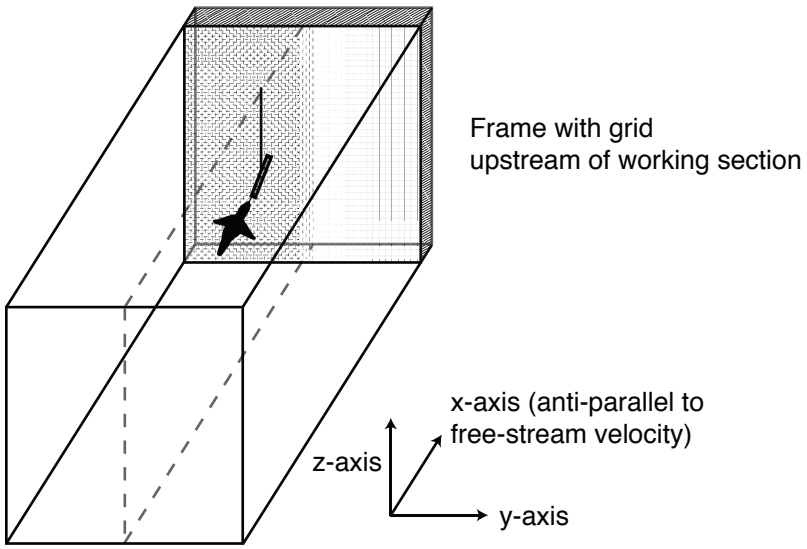

Figure 4.1. Set-up for asymmetric flow experiment, depicting the working section of the horizontal wind tunnel.

perturbations caused by the syringe's wake. We measured the velocity profile of both setups within a 13.3 cm × 17.7 cm region located 5 cm behind the upwind boundary, 2 cm below the level of the syringe, and laterally centered on the syringe using a particle image velocimetry (PIV) system (LaVision GmbH, Gottingen, Germany). For the uniform profile configuration, the mean streamwise velocity in the sub-region was 9.8±0.26 ms^{-1}. For the sheared profile configuration, the mean free-stream velocity was 4.2±0.12 ms^{-1} for the left half and 10.8±0.12 ms^{-1} for the right half, with the core of the high shear region centered about the inflection point across a distance of 6 cm (Figure 4.2).

Kinematic analysis

Each hummingbird had the following anatomical locations marked with non-toxic white paint prior to experiments: the wingtip (distal tip of last primary), the mid-leading wing edge (wrist), the mid-trailing wing edge (distal tip of 1st secondary), and the shoulder, of both the right and left wings, as well as the dorsal base of the tail. In order to obtain simultaneous, three-dimensional reconstructions of both wings, we recorded the hummingbirds using three synchronized high-speed cameras (HiSpec, Fastec Imaging, San Diego, CA, USA) positioned around the working section of the wind tunnel Images were acquired at a rate of 1000 frames s^{-1} with an exposure time of 1/2500 s, and only feeding bouts lasting longer than 3 seconds (~120 wingbeats) were analyzed in order to exclude transient flight kinematics from our dataset. Calibration of the cameras and three-dimensional feature tracking of the marked anatomical locations, as well as the birds' beak tips and bases, were all performed using the motion analysis software ProAnalyst 3-D Professional v.1.5.5.4 (Xcitex, Inc., Cambridge, MA, USA). Anatomical coordinates were subsequently exported and analyzed using custom algorithms written in MATLAB v.7.8 (Mathworks, Inc., Natick, MA, USA).

A bird-centered Cartesian coordinate system, with the origin centered at the base of the hummingbird beak (z-axis defined positive upward against gravity, x-axis defined positive downstream along the wind flow, and y-axis orthogonal to the other two axes) was used to describe the positions of the body and wings. We used the *z*-coordinate of the wrists to determine the frames containing downstroke and upstroke transitions for each wing, with instances of mid-upstroke and mid-downstroke determined as the frame halfway between half-stroke transitions. The downstroke and upstroke averages were computed for the following kinematic variables: wingbeat frequency (n), stroke amplitude (Φ), average wingtip angular velocity (ω), and average stroke plane angle (β), where the mean stroke planes for each wing were calculated by taking the first two principal components of the matrix consisting of the (mean-subtracted) shoulder and wingtip points.

In addition to the aforementioned downstroke and upstroke averaged variables, we also obtained measurements at each video frame of the following kinematic variables: chord angle (α_c), angle of attack (α), stroke position angle (φ), and wing deviation angle (θ). Chord angle was defined as the angle between the wing chord (the vector between the bird's mid-leading edge and mid-trailing edge) and the *X*-*Y* plane, with $\alpha_c>0°$

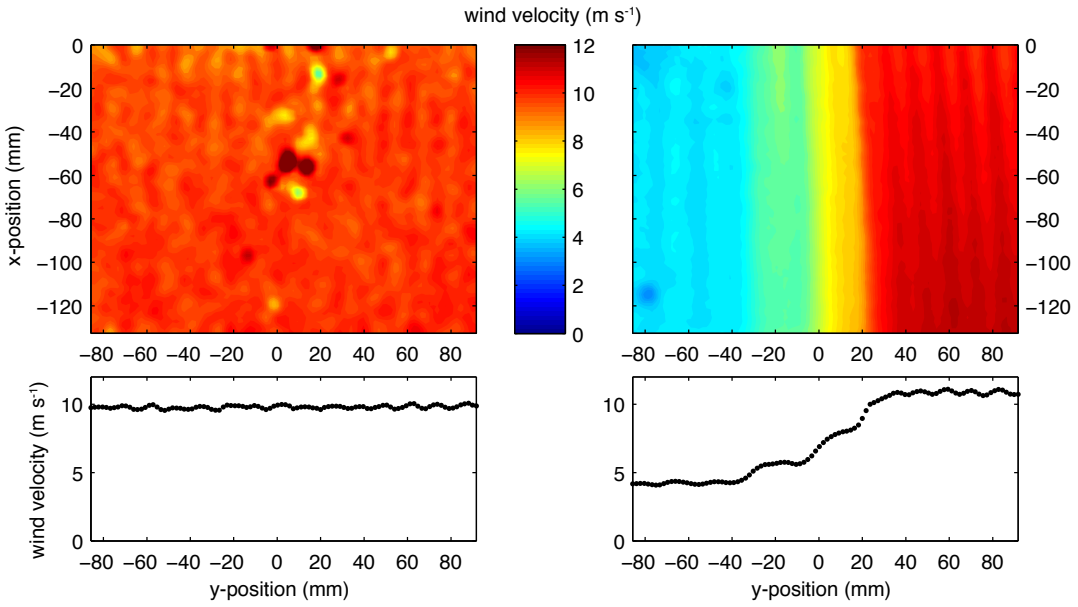

Figure 4.2. Velocity fields along the XY-plane in (left) uniform flow and (right) asymmetric flow.

indicating supination and $\alpha_c<0°$ indicating pronation. Angle of attack was defined as the angle between the wing chord and the resultant velocity vector, which was composed of the induced velocity (estimated from momentum jet theory [Johnson, 1980; Ellington, 1984], with the added assumption that the wings equally supported the mass of the bird), the free-stream velocity that each wing was exposed to (taken from PIV measurements), and the instantaneous flapping velocity (estimated by a finite difference method of the average of the wing's mid-leading edge and mid-trailing edge positions). We calculated the stroke position angle as the angular position of the shoulder to wingtip vector projected onto the mean stroke plane, with respect to the projection of the x-axis on the stroke plane, and the deviation angle as the angle between the shoulder to wingtip vector and the mean stroke plane (see Sane and Dickinson, 2001). We then linearly interpolated the chord angles, angles of attack, stroke position angles, and deviation angles, such that there were 100 points per wingbeat, and then subsequently calculated mid-downstroke (25% into wingbeat) and mid-upstroke (75% into wingbeat) values for the aforementioned variables.

Lastly, we assessed body roll by finding the angle between the left shoulder-to-right shoulder vector and its projection onto the *Y-Z* plane, and body yaw from the projection of the vector made of the shoulders' midpoint and the tail base onto the *X-Z* plane (see Ortega-Jimenez et al., 2014).

Statistical analysis

We performed paired t-tests comparing the mean values of each downstroke and upstroke variable between the left wing and the right wing, in order to determine whether there were any bilateral differences. These tests were done separately for the uniform flow condition and the asymmetric flow condition, with the null hypothesis being that there was no difference between the two wings for each variable in each condition. We also measured the average standard deviation of the wing kinematic variables of both wings (averaged between the wings), to determine if there was a statistical difference in variance. For measurements of kinematic variance, as well as body roll and body yaw, in which there was a single value for each flow condition, we again performed paired t-tests assessing whether the uniform flow value and the asymmetric flow value were significantly different. Prior to these tests, all of the variables were tested for normality with the Shapiro-Wilk test. Normality tests were performed in R (R Development Core Team, 2012), while all other statistical calculations were performed in Matlab.

Results

Despite the two-fold difference in the mean free-stream velocities encountered between their left and right wings, all hummingbirds were able to maintain stable flight as effortlessly in the asymmetric velocity profile as in the uniform velocity profile. Lateral, transverse, and dorsal representative wingtip and wrist trace projections from one bird are shown in Figure 4.3. Mid-stroke values of the kinematic variables for the left and right wings (averaged over the three birds) in both conditions, along with statistical

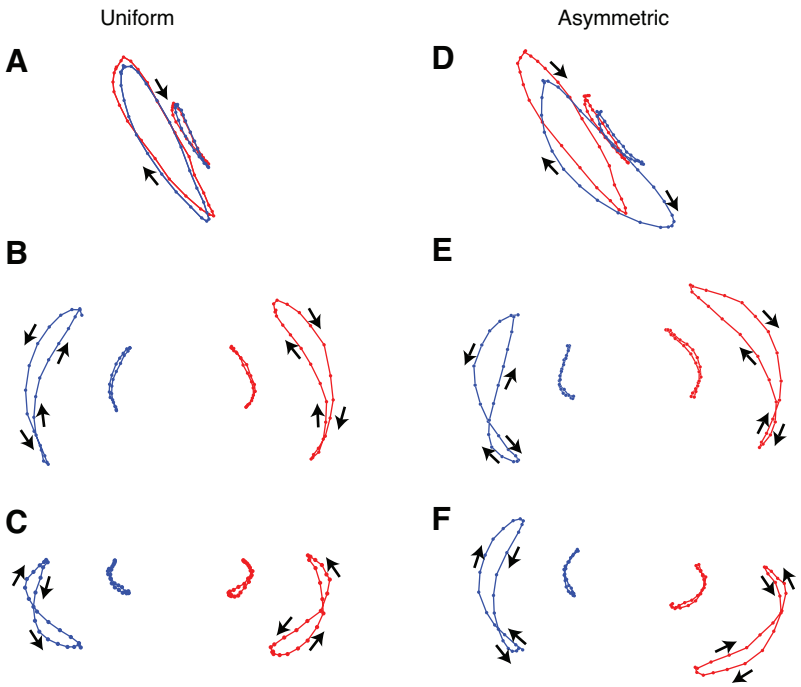

Figure 4.3. Example wingtip and mid-leading edge trajectories for one bird. Shown are the (A) lateral (i.e. in XZ-plane), (B) transverse (i.e. in YZ-plane), and (C) dorsal (i.e. in XY-plane) projections in uniform flow over one wingbeat, as well as the (D) lateral, (E) transverse, and (F) dorsal projections in asymmetric flow over one wingbeat. In the lateral view, bird is facing right; in transverse view, bird is facing into the page; in transverse view, bird is facing up. Left wing is depicted by blue traces, while right wing is depicted by red traces, with arrows indicating direction of wingtip movement.

	Uniform			Asymmetric		
	Left wing	Right wing	*p*	Left wing	Right wing	*p*
Φ_{ds} (°)[1]	**86.0 ± 27.2**	**91.5 ± 26.9**	**0.0295***	**87.7 ± 14.0**	**99.2 ± 15.8**	**0.0238***
Φ_{us} (°)	87.2 ± 26.8	91.7 ± 27.3	0.0854	**87.1 ± 14.9**	**98.3 ± 16.8**	**0.0339***
f_{ds} (Hz)	41.4 ± 2.0	39.6 ± 3.7	0.2264	43.6 ± 2.4	42.0 ± 0.5	0.3008
f_{us} (Hz)	40.3 ± 3.2	42.4 ± 1.7	0.2850	39.9 ± 3.4	41.7 ± 2.6	0.1702
ω_{ds} (rad s^{-1})	123.1 ± 32.9	124.3 ± 24.6	0.8289	134.5 ± 29.3	145.7 ± 24.6	0.0871
ω_{us} (rad s^{-1})	124.6 ± 32.2	135.2 ± 39.7	0.1404	133.5 ± 30.6	142.2 ± 19.2	0.3217
β_{ds} (°)	64.4 ± 3.7	65.2 ± 5.1	0.5414	55.4 ± 11.1	59.4 ± 2.7	0.4941
β_{us} (°)	59.9 ± 3.4	62.0 ± 5.2	0.3382	51.2 ± 11.4	56.2 ± 4.6	0.3366
φ_{ds}(°)	-8.8 ±11.1	-7.6 ±8.5	0.7822	2.4 ± 8.2	-12.5 ± 10.6	0.2669
φ_{us}(°)[2]	**-0.6 ±13.7**	**9.1 ±14.8**	**0.0362***	13.8 ± 9.5	-0.9 ± 12.7	0.2447
θ_{ds}(°)	9.0 ± 1.9	10.0 ± 4.5	0.5736	9.5 ± 0.8	10.8 ± 0.8	0.2900
θ_{us}(°)	-7.1 ± 0.6	-7.5 ± 2.6	0.8093	**-9.5 ± 1.3**	**-7.1 ± 1.7**	**0.0209***
$\alpha_{c,ds}$ (°)	-22.0 ± 3.6	-20.2 ± 10.2	0.6883	**-17.5 ± 10.6**	**-27.1 ± 11.6**	**0.0232***
$\alpha_{c,us}$ (°)	11.1 ± 7.3	14.0 ± 5.3	0.1482	27.3 ± 13.2	9.0 ± 7.5	0.1252
α_{ds} (°)	21.2 ± 2.2	24.0 ± 11.6	0.6824	**49.3 ± 6.1**	**19.2 ± 4.7**	**0.0092***
α_{us} (°)	11.3 ± 2.9	11.0 ± 1.2	0.8210	28.2 ± 10.8	11.1 ± 3.6	0.1622

Table 4.1. Means and standard deviations for stroke amplitude (Φ), wingbeat frequency (*f*), angular velocity (ω), stroke plane angle (β), mid-stroke chord angle (α_c), mid-stroke angle of attack (α), mid-stroke position angle (φ), and mid-stroke deviation angle (θ), in both downstroke (subscript 'ds') and upstroke (subscript 'us'), for Anna's hummingbirds flying in uniform and asymmetric flows (*N*=3). Paired t-test results for the aforementioned variables are also shown (d.f.=2); asterisked values in bold indicate *p*-value<0.05.

[1,2]Additional paired t-tests were performed to assess for statistically significant differences between uniform flow and asymmetric flow in the 'right–left' values of downstroke amplitude as well as mid-upstroke position angle; the resulting *p*-values were 0.0536 and 0.0919, respectively.

results, are given in Table 4.1; right-left differences in angle variables are also shown in Figure 4.3A. For the asymmetric flow condition, we found significant right-left differences in: downstroke amplitude (Φ_{ds}=87.7±14.0° and Φ_{ds}=99.2±15.8° for left and right wings, respectively; p=0.0238), upstroke amplitude (Φ_{ds}=87.1±14.9° and Φ_{ds}=98.3±16.8°; p=0.0339), mid-upstroke deviation angle (θ_{us}=-9.5±1.3° and θ_{us}=-7.1±1.7°; p=0.0209), mid-downstroke chord angle ($\alpha_{c,ds}$=-17.5±10.6° and $\alpha_{c,ds}$=-27.1±11.6°; p=0.0232), and mid-downstroke angle of attack (α_{ds}=49.3±6.1° and α_{ds}=19.2±4.7°; p=0.0092). In contrast, all of the variables, except Φ_{ds} and φ_{us}, were not significantly different between the wings in the uniform flow condition, with the right-left differences in both Φ_{ds} and φ_{us} not significantly differing between the two flow conditions (p=0.0536 and p=0.0919, respectively).

Plots of the wing orientation angles and attack angles of the left and right wings with respect to time for averaged over all the birds, in both the uniform and asymmetric flow conditions, are shown in Figure 4.5, where means and standard deviations of φ, θ, α_c, and α for both wings, as well as the means and standard deviations of the right-left wing difference, are plotted against wingbeat cycle. In the uniform flow condition, there was minimal asymmetry between the two wings in both magnitude and timing, with left and right wing extrema occurring simultaneously, and right-left differences centered at 0° throughout most of the wingbeat cycles. φ and θ had sinusoidal waveforms, with the wings moving back and forth predominantly within, and less so above or below, the mean stroke plane; φ ranged between -50° and 50° while θ ranged only between -10° and 10°, with maximum elevation above the plane occurring at mid-downstroke and maximum elevation below the stroke plane occurring at mid-upstroke. Throughout the wingbeat, chord angles followed a sinusoidal waveform as well, with α_c ranging from -25° to 25° and stroke reversals being relatively gradual and smooth. This resulted in positive values of the attack angle throughout the wingbeat cycle for both wings, with maximum values occurring at the downstroke-to-upstroke transition.

By contrast, wing asymmetries could be observed in the asymmetric flow condition, particularly in deviation, chord, and attack angles. While the wings differed in stroke position angle, with the right wing more posterior than the left wing throughout much of the wingbeat cycle and particularly around the upstroke-to-downstroke reversal, these differences were generally insignificant. In contrast, while the left wing's deviation angle had a typical sinusoidal waveform, with the downstroke approximately equal and opposite to the upstroke, distinct differences existed between the two half-strokes for the right wing's deviation angle. Additionally, right-left differences in θ were not centered at zero throughout the wingbeat cycle, but rather oscillated between negative and positive values. Maximum values of chord angle differed between the two wings, with α_c reaching 32.9±16.1° and 18.7±7.7° for the left and right wings, respectively. We observed slight timing differences between the two wings as well, with wings reaching minima and maxima during the downstroke and upstroke, respectively, at different times. However, when cross-correlation analysis assessing for delays between the two wings' angle measurements was performed, the results were inconsistent between birds. In two

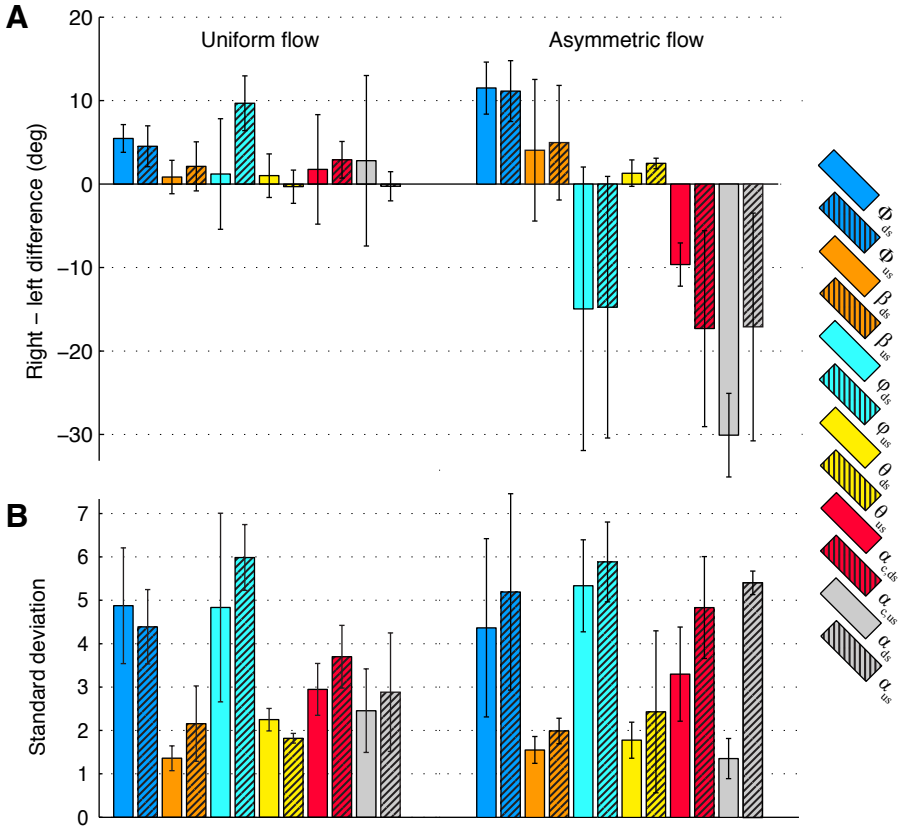

Figure 4.4 (A) Differences (right – left) between the two wings and (B) mean standard deviation (averaged between both wings, over 4-5 wingbeats), for stroke amplitude (Φ), stroke plane angle (β), mid-stroke position angle (φ), mid-stroke deviation angle (θ), mid-stroke chord angle (α_c), and mid-stroke angle of attack (α), in both downstroke (subscript 'ds') and upstroke (subscript 'us'), for Anna's hummingbirds flying in uniform and asymmetric flows (N=3 birds). Error bars denote 1 s.d.

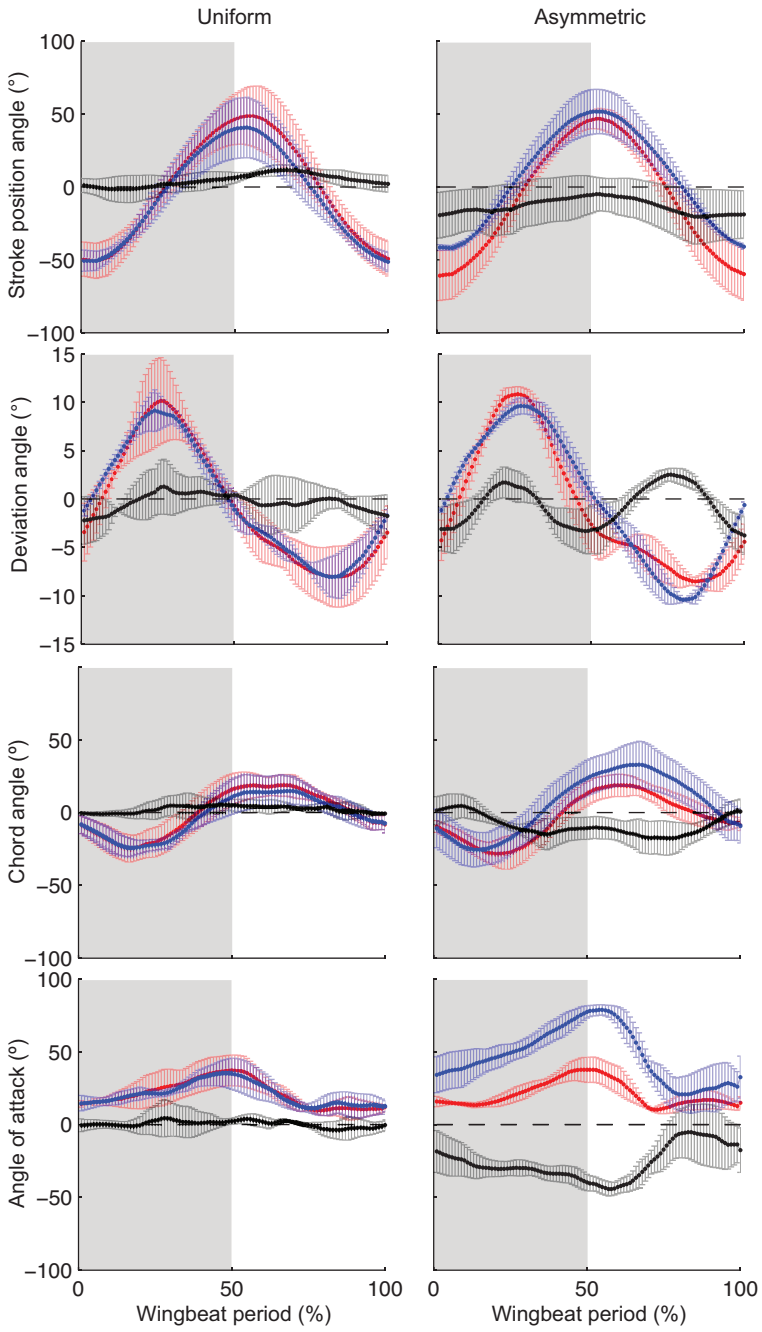

Figure 4.5 Average stroke position angle, deviation angle, chord angle, and angle of attack throughout one wingbeat period (*N*=3 birds, 4-5 wingbeats per bird) for Anna's hummingbirds flying in uniform flow and asymmetric flow, respectively. Gray regions denote downstroke while white regions denote upstroke, with stroke transitions identified by the vertical (z-component) of wrist motion. Red plots indicate the right wing, blue plots indicate the left wing, and black plots indicate the difference between the two wings (*right – left*), with all values as mean ± 1 s.d. The horizontal dashed line indicates a value of 0°.

	Uniform	Asymmetric	*p*
Body yaw (°)	1.6 ± 0.7	4.0 ± 3.0	0.3771
Body roll (°)	2.9 ± 0.2	3.9 ± 1.5	0.4174

Table 4.2. Means and standard deviations for body yaw and body roll, for Anna's hummingbirds flying in uniform and asymmetric flows (*N*=3). Positive values of yaw connote counter-clockwise rotation about the z-axis, while positive values of roll connote counter-clockwise rotation about the x-axis. Paired t-test results for the aforementioned variables are also shown (d.f.=2).

	Uniform	Asymmetric	*p*
Φ_{ds} (°)[1]	4.9±1.3	4.4 ± 2.0	0.7963
Φ_{us} (°)[2]	4.4±0.9	5.2 ± 2.3	0.6997
f_{ds} (Hz)	2.2±0.4	2.1 ± 2.0	0.9170
f_{us} (Hz)	2.3±0.8	2.1 ± 0.8	0.3715
ω_{ds} (rad s^{-1})	10.7±2.9	12.3 ± 0.8	0.5150
ω_{us} (rad s^{-1})	6.6±1.6	9.8 ± 3.6	0.1051
β_{ds} (°)	1.4±0.3	1.6 ± 0.3	0.6263
β_{us} (°)	2.2±0.9	2.0 ± 0.3	0.6705
φ_{ds}(°)	4.8±2.2	5.3 ± 1.1	0.6829
φ_{us}(°)	6.0±0.8	5.9 ± 0.9	0.9005
θ_{ds}(°)	2.2±0.3	1.8 ± 0.4	0.2707
θ_{us}(°)	1.8±0.1	2.4 ± 1.9	0.6468
$\alpha_{c,ds}$ (°)	2.9±0.6	3.3 ± 1.1	0.6374
$\alpha_{c,us}$ (°)	3.7±0.7	4.8 ± 1.2	0.4074
α_{ds} (°)	2.5±1.0	1.4 ± 0.5	0.1785
α_{us} (°)	2.9±1.4	5.4 ± 0.3	0.0638

Table 4.3. Mean variation of kinematic variables averaged between both wings (*N*=3), for uniform flow and asymmetric flow, and paired t-test results (d.f.=2).

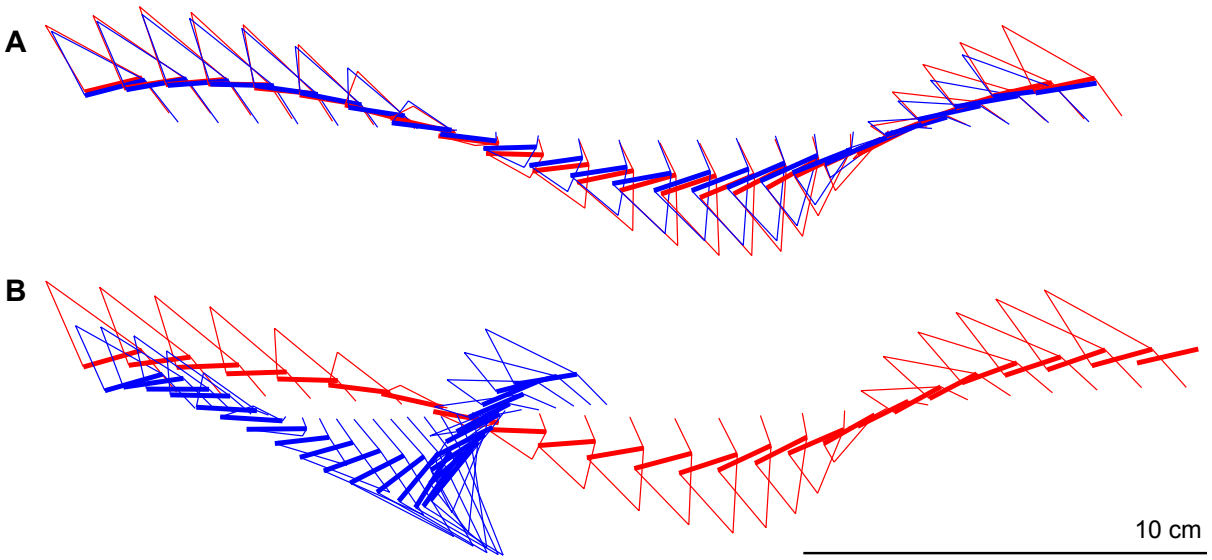

Figure 4.6. Representative lateral projections of the wingtip, shoulder, and chord (thick line) for left (blue color) and right (red color) wings over one wingbeat, with translation due to the free-stream velocity and time. Center of bird is moving from left to right. (A) contains the projections in the uniform flow, while (B) contains the projections in the asymmetric flow.

subjects, the left wing lagged behind the right wing, with a normalized delay of ~13% of the wingbeat period; however, in the third subject, the left wing led the right wing, with a similar magnitude. Despite these inconsistencies, the absolute asymmetries in the chord angle, coupled with the sheared wind profile, resulted in drastic differences in the angle of attack between the two wings. As in the uniform flow profile, angles of attack were positive for both wings throughout the entire wingbeat, and the two wings generally followed similar patterns, reaching maximum values near the onset of upstroke. However, the left wing exhibited higher values of α than the right wing for the entirety of the wingbeat, particularly at mid-downstroke and at supination; at mid-upstroke, in contrast, the left and right wings' attack angles were not significantly different from one another.

Values and statistical results assessing for differences between the uniform flow and the asymmetric flow in body yaw and body roll are presented in Table S4.2, while values and statistical results for standard deviation in Φ_{ds}, Φ_{us}, f_{ds}, f_{us}, ω_{ds}, ω_{us}, β_{ds}, β_{us}, φ_{ds}, φ_{us}, θ_{ds}, θ_{us}, $\alpha_{c,ds}$, $\alpha_{c,us}$, α_{us}, and α_{ds} are shown in Table S4.3 and Fig. 6. Overall, we found no significant difference in any of the aforementioned body and wing kinematic variables between the two flow conditions. Both body roll and yaw angles were minimal in either flow, ranging from 1.6± 0.7° to 4.0±3.0°, while variance in wing kinematic variables did not significantly increase from the uniform flow condition to the asymmetric flow condition.

Discussion

Calypte anna maintained stable forward flight within a sharp velocity gradient by partially decoupling the movements of their two wings throughout the wingbeat; in contrast, the kinematics measured under uniform flow configurations were characterized by much greater bilateral symmetry. To maintain a stable equilibrium within the asymmetric flow, the hummingbird must concurrently overcome the force moment induced by unbalanced drag forces on either side by producing an opposing yaw torque of equal magnitude as well as maintain identical lift production on both sides to inhibit body roll. Moreover, the hummingbird was obliged to contend with the flow perturbations generated by the plane mixing-layer. Although turbulent fluctuations were generally weak in the measurement region (with turbulent intensity $u'/U<0.1$), vortex instabilities, like those produced at the core of the mixing-layer, can potentially increase the energetic cost of flight by markedly impacting the wingbeat kinematics and metabolic rates of volant animals (Combes and Dudley, 2009). For example, while flying in the wakes behind cylinders of varying diameters, hummingbirds exhibited increasing variability in their wingbeat frequencies with increasing cylinder size and wind speed (Ortega-Jimenez et al., 2014). The relatively invariant standard deviations of kinematic variables between the uniform and asymmetric flow condition suggest the mixing-layer vortices were likely small relative to the wingspan of the hummingbirds and thus had negligible influence on wing kinematics in comparison to the velocity asymmetry itself. Given that both the strength and size of mixing-layer vortices grow with distance downstream of an initial instability (Brown & Roshko, 1974), the close proximity of the

mesh screen to the syringe may have mitigated possible interactions between the birds and those large vortices capable of impairing flight performance.

Unlike in free-flight turns, the hummingbirds were not required to produce laterally oriented centripetal forces. Thus while the asymmetric flow configuration posed a flight challenge without a direct analog outside of the laboratory, our experiment did elicit interesting response behavior from the birds that has expanded our understanding of the hummingbird's ability to independently articulate its wings to produce and manipulate aerodynamic forces beyond normal demands.

Several aspects of the compensatory responses to asymmetric flow were consistent with previous observations describing kinematics to various flight demands. The asymmetric modulation of stroke amplitude seen in this study, for example, was an expected response to differing power demands, as stroke amplitude modification is the primary mechanism by which hummingbirds modulate aerodynamic forces (Chai and Dudley, 1995; Chai et al., 1997; Altshuler and Dudley, 2002; Altshuler and Dudley, 2003). Expansion of the faster (outer) wing's stroke amplitude was also observed for *C. anna* performing pure yaw turns while hovering (Altshuler et al., 2012) as well as for fruit flies (*Drosophila melanogaster*) performing both free flight saccades (Fry et al., 2003) and sashay maneuvers (Ristroph et al., 2009). The symmetry of both wingbeat frequency and angular velocity between the left and right wings is also consistent with previous related studies. For example, Tobalske et al. (2007) found considerable overlap in both wingbeat frequency and wingtip speed of similarly sized rufous hummingbirds (*Selasphorus rufus*) engaged in forward flight at speeds ranging from 2 to 12 m s^{-1}, a range which covers the different speeds in the asymmetric flow condition in our study, while Altshuler et al. (2012) found no significant differences between yawing flight and normal hovering flight in hummingbirds for either wingbeat frequency or wingtip speed, as well.

As aerodynamic forces depend upon the relative velocity vector, and it is the flight velocity that increasingly dominates the relative velocity at moderate to fast speeds, we would expect changes in the wings' position and orientation angles (i.e. mean stroke plane, stroke position, deviation, and chord/pitch) to be more effective than changes in wingtip speed for modulating lift and drag forces. Interestingly, we did not observe significant differences in stroke plane angle between the wings in the asymmetric flow condition. In contrast, the outer wing has a higher upstroke stroke plane angle than the inner wing for hummingbirds engaged in slow yawing turns (Altshuler et al., 2012), while the stroke plane angle increases with increasing flight speed for hummingbirds engaged in uniform forward flight (Tobalske et al., 2007); thus, we would expect to see greater values of both β_{us} and β_{ds} for the right wing than the left wing in the asymmetric flow condition in our study. In studies of insect flight, however, both β_{us} and β_{ds} have been found to be lower for the outer wing than the inner wing for fruit flies engaged in relatively fast, free flight yaw maneuvers (Fry et al., 2003). Additionally, in a study of sharp yaw turns in fruit flies, Bergou et al. (2010) observed that asymmetries in the wings' stroke plane angles do not cause any new yawing torques at all – but rather merely reorient the already existing forces about the yaw axis. Although direct comparisons

between the flights of fruit flies and hummingbirds are complicated by species-specific disparities in average Reynolds number and morphology, this finding, in conjunction with our additional observation that subjects in our study differed as to which wing had the higher stroke plane angle than the other, suggests that asymmetries in stroke plane angle are not necessary for producing the unequal aerodynamic forces required in this study. Rather, the wings of hummingbirds are articulate enough such that they need only to dramatically manipulate their orientation within the stroke plane.

Indeed, although differences in stroke position angle were either insignificant or inconsistent with respect to mid-stroke magnitudes as well as periodic shifts/delays, left and right wings differed in both deviation angle and chord angle values throughout the majority of the wingbeat. With greater sampling size, we expect that the statistical significance of right-left angle differences would be greater in both half-strokes, rather than just within the downstroke, as we currently observe. Regardless, absolute chord angles for the right wing, in comparison to the left wing, were drastically larger at mid-downstroke and drastically smaller at mid-upstroke, resulting in even greater differences between the wings' angles of attack, with greater values of α for the left wing than the right wing in both half-strokes in the asymmetric flow condition. Values of $\boldsymbol{\alpha}$ for the left wing were much higher than expected, particularly when compared to *S. rufus* engaged in uniform forward flight at a similar speed. At mid-downstroke, for example, α_{ds}=49.3±6.1° for the left wing in the asymmetric flow condition in our study, while α_{ds}~15° for *S. rufus* (Tobalske et al., 2007). The extremely large angle of attack entails that a substantial area of the wing is facing the flow, causing it to act less effectively as an airfoil and more as a drag-generating body. Similar results were also found in studies of fruit flies performing lateral accelerations, with right-left differences achieved through slight periodic shifts between the wings (Ristroph et al., 2009; Bergou, et al., 2010); however, fruit flies performing other yawing maneuvers were observed to have the opposite trend as well, with larger attack angle values for the outer wing compared to the inner wing (Fry et al., 2003).

In a study examining the aerodynamic forces of a revolving hummingbird's wing at Reynolds number Re=5×10^4, attack angles of α=50° and 20° were associated with lift/drag coefficients ratios of ~4 and ~10, respectively (Altshuler et al., 2004). Given the similar values of Reynolds number and α in our study and Altshuler et al. (2004), a substantial modification in just the angle of attack appears to generate sufficient aerodynamic torque to overcome the two-fold difference in airspeeds. Considering that bilateral differences in angular velocity, stroke plane angle, and stroke amplitude were either minimal or non-existent in the asymmetric flow condition, a case can be made that the principal kinematic response to asymmetric force requirements at high speeds is to simply adjust wing rotation throughout the wingbeat, primarily at mid-downstroke, and therefore leverage the effectiveness of lift/drag modulation via angle of attack. Even in the extreme asymmetric flow condition hummingbirds were challenged with in our study, this subtle kinematic modification was sufficient.

Finally, contrary to predictions, there was neither body roll nor body yaw in the asymmetric flight condition. While banking and rolling are required in the production of

lateral forces for fixed wing aircrafts (Ristroph et al., 2009), many volant animals such as pigeons and bats also require an alteration in body orientation in order to perform lateral turns (Ros et al., 2011; see references in Ros et al., 2011 and Altshuler et al., 2012). In contrast, fruit flies can perform such maneuvers by generating a pure yaw torque similar to hummingbirds (Bergou et al., 2010; Ristroph et al., 2009) as well as through a combination of changing body roll and pitch angles (Muijeres et al., 2014) depending upon the speed of the maneuver. Previously, Altshuler et al. (2012) found that hummingbirds are able to redirect aerodynamic force vectors without having to concurrently reorient body position, and our study lends further evidence to that conclusion. Nonetheless, our results are surprising as the angular speeds involved are quite different between the two studies, with this study requiring a much greater asymmetry in lateral force production. All of these results suggest that agility, in terms of rotational accelerations and maneuvers, is probably both size-dependent and species-specific.

REFERENCES

Aldridge, H. D. J. N. 2009. Flight kinematics and energetics in the little brown bat, *Myoris lucifugus* (Chiroptera: Vespertilionidae), with reference to the influence of ground effect. *J. Zool*. **216**, 507–5 17. (DOI 10.1111/j.1469-7998.1988.tb02447.x)

Alexander, D. E. 2004. Nature's flyers: birds, insects, and the biomechanics of flight. Johns Hopkins University Press.

Altshuler, D. L. & Dudley, R. 2002. The ecological and evolutionary interface of hummingbird flight physiology. *J Exp Bio* **205**, 2325–2336.

Altshuler, D. L. & Dudley, R. 2003. Kinematics of hovering hummingbird flight along simulated and natural elevational gradients. *J Exp Bio* **206**, 3139–3147.

Altshuler, D. L., Stiles, F. G. & Dudley, R. 2004*a*. Of Hummingbirds and Helicopters: Hovering Costs, Competitive Ability, and Foraging Strategies. *Am Nat* **163**, 16–25

Altshuler, D. L., Dudley, R. & Ellington, C. P. 2004*b*. Aerodynamic forces of revolving hummingbird wings and wing models. *J. Zool.* **264**, 327-332. (DOI 10.1017/S0952836904005813)

Altshuler, D. L., Princevac, M., Pan, H. & Lozano, J. 2009. Wake patterns of the wings and tail of hovering hummingbirds. *Exp. Fluids* **46**, 835–846. (DOI 10.1007/s00348-008-0602-5)

Altshuler, D. L, Dudley, R., Heredia, S. M. and McGuire, J. A. (2010). Allometry of hummingbird lifting performance. *J. Exp. Biol.* 213, 725-734.

Altshuler, D. L., Quicazan-Rubio, E. M., Segre, P. S. & Middleton, K. M. 2012. Wingbeat kinematics and motor control of yaw turns in Anna's hummingbirds (Calypte anna). *J Exp Biol.* **215**, 4070–4084.

Askew, G. N., Marsh, R. L., & Ellington, C. P. 2001. The mechanical power output of the flight muscles of the blue-breasted quail (*Coturnix chinensis*) during take-off. *J. Exp. Biol.* **204**, 3601-3619.

Azuma, A., Azuma, S., Watanabe, I., and Furuta, T. 1985. Flight mechanics of a dragonfly. *J. Exp. Biol.* **116**, 79-107.

Bartholomew, G. A. & Lighton, J. R. 1986. Oxygen consumption during hover-feeding in free-ranging Anna's hummingbirds. *J. Exp. Biol.* **123**, 191-199.

Berg, A. M. and Biewener, A. A. 2008. Kinematics and power requirements of ascending and descending flight in the pigeon (Columba livia). *J. Exp. Biol*. 211, 1120-1130.

Bergou, A. J., Ristroph, L., Guckenheimer, J., Cohen, I. & Wang, Z. J. 2010. Fruit Flies Modulate Passive Wing Pitching to Generate In-Flight Turns. *Phys. Rev. Lett.* **104**

Blake, R.W. 1979. The energetics of hovering in the mandarin fish (*Synchropus picturatus*). *J. Exp. Biol.* **82**, 25-33.

Brobeck, J. R. & Dubois, A. B. 1980. Energy exchange. In *Medical Physiology*, vol. II (ed. V. B. Mountcastle), pp. 1351-1365. St Louis: D. V. Mosby Co.

Brown, G. L. & Roshko, A. 1974. On density effects and large structure in turbulent mixing layers. *J Fluid Mech* **64**, 775.

Chai, P. & R. Dudley. 1995. Limits to vertebrate locomotor energetics suggested by hummingbirds hovering in heliox. *Nature* **377**, 722-725.

Chai P. & Dudley R. 1996 Limits to flight energetics of hummingbirds hovering in hypodense and hypoxic gas mixtures. *J. Exp. Biol*. **199**, 2285–2295.

Chai, P. & Millard, D. 1997. Flight and size constraints: hovering performance of large hummingbirds under maximal loading. *J. Exp. Biol.* **200**, 2757-2763.

Chai, P., Chen, J. & Dudley, R. 1997. Transient hovering performance of hummingbirds under conditions of maximal loading. *J Exp Bio* **200**, 921–929.

Cheeseman, I. C. and Bennett, W. E. 1955 *The effect of the ground on a helicopter rotor in forward flight*. Aeronaut. Res. Counc. (U.K.) Technical Report, R & M No. 3021.

Clark, C. J. 2006. Observations on the Vervain hummingbird's (*Mellisuga minima*) display dive and territorial behavior. *Ornitologia Neotropical* **17**, 403-408.

Clark, C. J. 2009. Courtship dives of Anna's hummingbirds offer insights into flight performance limits. *Proc. Roy. Soc. B* **276**, 3047-3052.

Clark, C. J. and Dudley, R. 2010. Hovering and forward flight energetics in Anna's and Allen's hummingbirds. *Physiol. and Biochem. Zool.* **83**, 654-652.

Clark, C. J., Feo, T. J., and Escalante, I. 2011. Courtship displays and natural history of Scintillant (*Selasphorus scintilla*) and Volcano (*S. flammula*) hummingbirds. *Wilson Journal of Ornithology* **123**, 218-228.

Combes, S. A. & Dudley, R. 2009. Turbulence-driven instabilities limit insect flight performance. *P Natl Acad Sci USA* **106**, 9105–9108.

Dial, K. P. and Biewener, A. A. 1993. Pectoralis muscle force and power output during different modes of flight in pigeons (*Columba livia*). *J. Exp. Biol.* **176**, 31-54.

Dudley, R. 2000 *The biomechanics of insect flight: form, function, evolution*. Princeton: Princeton University Press

Dudley, R. 2002. Mechanisms and Implications of Animal Flight Maneuverability. *Integr Comp Bio* **42**, 135–140.

Ellington, C. P. 1984*a*. The aerodynamics of hovering insect flight. I. The quasi-steady analysis. *Phil. Trans. R. Soc. B* **305**, 1-15.

Ellington, C. P. 1984*b*. The aerodynamics of hovering insect flight. II. Morphological paramters. *Phil. Trans. R. Soc. B* **305**, 17-40.

Ellington, C. P. 1984*c*. The aerodynamics of hovering insect flight. III. Kinematics. *Phil. Trans. R. Soc. B* **305**, 41-78.

Ellington, C. P. 1984*d*. The aerodynamics of hovering insect flight. IV. Aerodynamic mechanisms. *Phil. Trans. R. Soc. B* **305**, 79-113.

Ellington, C. P. 1984*e*. The aerodynamics of hovering insect flight. V. A vortex theory. *Phil. Trans. R. Soc. B* **305**, 114-144.

Ellington, C. P. 1984*f*. The aerodynamics of hovering insect flight. VI. Lift and power requirements. *Phil. Trans. R. Soc. B* **305**, 145-181.

Epting, R. J. 1980. Functional Dependence of the Power for Hovering on Wing Disc Loading in Hummingbirds. *Physiol Zoo* **53**, 347–357.

Evangelista, D., Cam, S., Huynh, T., Kwong, A., Mehrabani, H., Tse, K., and Dudley, R. (2014). Shifts in stability and control effectiveness during evolution of Paraves support aerial maneuvering hypothesis for flight origins. *Peer J* 2:e632; DOI 10.7717/peerj.632

Feinsinger, P. 1977. Notes on the hummingbirds of Monteverde, Cordillera Tilaran, Costa Rica. *Wilson Bull* **89**, 159-164.

Finn, J., Carlsson, J., Kelly, T. & Davenport, J. 2012 Avoidance of headwinds or exploitation of ground effect—why do birds fly low? *J. Field Ornithol.* **83**, 192–202. (DOI 10.1111/j.1557-9263.2012.00369.x)

Fradenburgh, E. A. 1960 The helicopter and the ground effect machine. *J. Am. Helicopter Soc.* **5**, 26–28.

Fry, S. N., Sayaman, R. & Dickinson, M. H. 2003. The aerodynamics of free-flight maneuvers in Drosophila. *Science* **300**, 495–498.

Gao T. & X. Lu 2008. Insect normal hovering flight in ground effect. *Phys. Fluids* **20**, 087101-1-11. (DOI 10.1063/1.2958318)

Glauert, H. 1983. The elements of aerofoil and airscrew theory. Cambridge: Cambridge University Press. 219-220.

Green, R. B., Gillies, E. A. and Brown, R. E. 2005. The flow field around a rotor in axial descent. *J. Fluid Mech.* **534**, 237-261.

Greenewalt, C. H. 1960. *Hummingbirds*. (Courier Dover Publications).

Hayden, J. S. 1976 *The effect of the ground on helicopter hovering power required*. 32nd American Helicopter Society Forum, Washington, DC.

Hedenstrom, A. and Liechti, F. 2001. Field estimates of body drag coefficient on the basis of dives in passerine birds. *J. Exp. Biol*. **204**, 1167-1175.

Hedrick, T. L., Usherwood, J. R. & Biewener, A. A. 2007. Low speed maneuvering flight of the rose-breasted cockatoo (Eolophus roseicapillus). II. Inertial and aerodynamic reorientation. *J Exp Bio* **210**, 1912–1924.

Hughes, P. M. & Rayner, J. M. V. 1991. Addition of artificial loads to long-eared bats *Plecotus auritus*: handicapping flight performance. *J. Exp. Biol.* **161**, 285-298.

Iriarte-Díaz, J. & Swartz, S. M. 2008. Kinematics of slow turn maneuvering in the fruit bat Cynopterus brachyotis. *J Exp Bio* **211**, 3478–3489.

Johansen, K., Berger, M., Bicudo, J. E. P. W., Ruschi, A. and De Almeida, P. J. (1987). Respiratory properties of blood and myoglobin in hummingbirds. *Physiol. Zool.* **60**, 269-278.

Johnson, W. 1980 *Helicopter theory*. New York: Dover Press.

Kim, E. J., Wolf, M., Ortega-Jimenez, V. M., Cheng, S. H. & Dudley, R. 2014. Hovering performance of Anna's hummingbirds (*Calypte anna*) in ground effect. *J Roy Soc Interface* **11**, 20140505–20140505.

Lasiewski, R. C. and Dawson, W. R. (1967). A re-examination of the relation between standard metabolic rate and body weight in birds. *Condor*. **69**, 13-23.

Lawrence, M. A. 2013. ez: Easy analysis and visualization of factorial experiments. R package version 4.2-2.

Leishman, J. G. 2006 *Principles of helicopter aerodynamics*, 2nd ed. Cambridge: Cambridge University Press.

Light, J. S. 1993 Tip vortex geometry of a hovering helicopter rotor in ground effect. *J. Am. Helicopter Soc.* **38**, 34–42.

Lighthill, M.J. 1979 A simple fluid flow model of ground effect on hovering. *J. Fluid*

Mech. **93**, 781–797.

Lima, S. L. 1991 Energy, predators, and the behaviour of feeding hummingbirds. *Evol. Ecol.* **5**, 220–230.

MacAyeal, L. C., Riskin, D. K., Swartz, S. M. and Breuer, K. S. 2011. Climbing flight performance and load carrying in lesser dog-faced fruit bags (Cynopterus brachyotis). *J. Exp. Biol*. **214**, 786-793.

Maeda, M. & Liu, H. 2013 Ground effect in fruit fly hovering: a three-dimensional computational study. *J. Biomech. Sci. Eng.* **8**, 344-355. (DOI 10.1299/jbse.8.344)

Morris, C. R., Nelson, F. E., & Askew, G. N. 2010 The metabolic power requirements of flight and estimations of flight muscle efficiency in the cockatiel (*Nymphicus hollandicus*). *J. Exp. Biol.* **213**, 2789-2796. (DOI 10.1242/jeb.035717)

Muijres, F. T., Elzinga, M. J., Melis, J. M. & Dickinson, M. H. 2014. Flies Evade Looming Targets by Executing Rapid Visually Directed Banked Turns. *Science* **344**, 172–177.

Nathan, N.D. & Green, R.B. 2012 The flow around a model helicopter main rotor in ground effect. *Exp. Fluids* **52**, 151-166. (DOI 10.1007/s00348-011-1212-1)

Norberg, U. M. 1990 *Vertebrate flight*. Berlin: Springer Verlag.

Nowroozi, B. N., Strother, J. A., Horton, J. M., Summers, A. P., & Brainerd, E. L. 2009 Whole-body lift and ground effect during pectoral fin locomotion in the northern spearnose poacher (*Agonopsis vulsa*). *Zoology (Jena)* **112**: 393-402. (DOI 15.1016/j.zool.2008.10.005)

Ortega-Jiménez, V. M. & Dudley, R. 2012 Flying in the rain: hovering performance of Anna's Hummingbirds under varied precipitation. *Proc. R. Soc. B* **279**, 3996-4002. (DOI 10.1098/rspb.2012.1285.)

Ortega-Jimenez, V. M., Sapir, N., Wolf, M., Variano, E. A. & Dudley, R. 2014. Into turbulent air: size-dependent effects of von Karman vortex streets on hummingbird flight kinematics and energetics. *P R Soc B* **281**, 20140180–20140180.

Park, H. & Choi, H. 2010 Aerodynamic characteristics of flying fish in gliding flight. *J. Exp. Biol*. **213**, 3269–3279. (DOI 10.1242/jeb.046052)

Pearson, O. P. 1950. The metabolism of hummingbirds. *Condor*. **52**, 145-152.

Pennycuick, C. J. 1968. Power requirements for horizontal flight in the pigeon *Columba livia*. *J. Exp. Biol.* **49**, 527-555.

Pennycuick, C. J. 1975. Mechanics of flight. In Avian Biology, vol. 5 (ed. D. S Farner and J. R. King), pp. 1-75. London: Academic Press.

Pennycuick, C. J. & Rezende, M. A. 1984. The specific power output of aerobic muscle, related to the power density of mitochondria. *J. Exp. Biol.* **108**, 377-392.

Pennycuick, C. J., Fuller, M. R. and McAllister, L. (1989). Climbing performance of Harris' hawks (Parabuteo unicinctus) with added load: implications for muscle mechanics and for radiotracking. *J. Exp. Biol*. **142**, 17-29.

Pereira, J. C. F., Maia, N., & Pereira, J. M. C. 2009 A computational fluid dynamics study of a 2D airfoil in hovering flight under ground effect. *CMES-Comp. Model. Eng.* **49**, 113-141.

Pournazeri, S., Segre, P. S., Princevac, M., & Altshuler, D. L. 2013 Hummingbirds generate bilateral vortex loops during hovering: evidence from flow visualization. *Exp. Fluids* 54: 1-11. (DOI 10.1007/s00348-012-1439-5)

Price, J. "Downtown Raleigh's chimney swifts could teach drones to fly in flocks." Newsobserver.com. 1 Oct. 2014. Web. 26 Oct. 2014.

Rayner, J.M.V. 1991 On the aerodynamics of animal flight in ground effect. *Phil. Trans. R. Soc. Lond. B.* **334**, 119-128. (doi: 10.1098/rstb.1991.0101)

Rayner, J. M. V. & Thomas, A. L. R. 1991 On the vortex wake of an animal flying in a confined volume. *Phil. Trans. R. Soc. B* **33**, 107–117.

Rayner, J. M. V. 1994 Aerodynamic corrections for the flight of birds and bats in wind tunnels. *J. Zool*. **234**, 537-563.

Ristroph, L., Berman, G. J., Bergou, A. J., Wang, Z. J. & Cohen, I. 2009. Automated hull reconstruction motion tracking (HRMT) applied to sideways maneuvers of free-flying insects. *J Exp Bio* **212**, 1324–1335.

Ros, I. G., Bassman, L. C., Badger, M. A., Pierson, A. N. & Biewener, A. A. 2011. Pigeons steer like helicopters and generate down- and upstroke lift during low speed turns. *P Natl Acad Sci USA* **108**, 19990–19995.

Rozhdestvensky, K.V. 2000 *Aerodynamics of a lifting system in extreme ground effect,* 1st edn. Springer-Verlag, Berlin.

Sane, S. P. & Dickinson, M. H. 2001. The control of flight force by a flapping wing: Lift and drag production. *J Exp Biol.* **204**, 2607–2626.

Stack, J., Caradonna, F. X. and Savas, O. 2005. Flow visualizations and extended thrust time histories of rotor vortex wakes in descent. 4th American Helicopter Society Decennial Specialists' Conference on Aeromechanics, San Francisco, CA, USA, 21–23 January.

Stiles, F. G. 1982. Aggressive and courtship displays of the male Anna's hummingbird.

Condor **84**, 208-225.

Stiles, F. G. 1995 Behavioral, ecological and morphological correlates of foraging for arthropods, by the hummingbirds of a tropical wet forest. *Condor* **97**, 853–878.

Su, J-Y, Ting, S-C, Chang, Y-H, & Yang, J-T. 2012. A passerine spreads its tail to facilitate a rapid recovery of its body posture during hovering. *J. R. Soc., Interface* **9**, 1674-1684. (DOI 10.1098/rsif.2011.0737)

Suarez, R. K, Brown, G. S., & Hochachka, P. W. 1986 Metabolic sources of energy for hummingbird flight. *Am. J. Physiol.* **251,** R537-R542.

Taylor, G. K. & Thomas, A. 2002. Animal flight dynamics II. Longitudinal stability in flapping flight. *J Theor Biol* **214**, 351–370.

Thompson, B. C. 1977. Behavior of Vaux's swifts nesting and roosting in a chimney. *The Murrelet*. **58**, 73-77.

Tobalske, B. W., Altshuler, D. L. and Powers, D. R. 2004. Take-off mechanics in hummingbirds (Trochilidae). *J. Exp. Biol*. **207**, 1345-1352.

Tobalske, B. W. Biomechanics of bird flight. 2007. *J Exp Bio* **210**, 3135–3146.

Tobalske, B. W., Warrick, D. R., Clark, C. J., Powers, D. R., Hedrick, T. L, Hyder, G. A., & Biewener, A. A. 2007 Three-dimensional kinematics of hummingbird flight. *J. Exp. Biol.* **210**:,2368-2382. (DOI 10.1242/jeb.005686)

Truong,T.V., Yoon, K.J., Park, H.C. Kim, M. J., & Byun, D.Y. 2013 Aerodynamic forces and flow structures of the leading edge vortex on a flapping wing considering ground effect. *Bioinspir. Biomim.* **8**, 036007. (DOI:10.1088/1748-3182/8/3/036007)

Tucker, V. A. 1968. Respiratory exchange and evaporative water loss in the flying budgerigar. *J. Exp. Biol.* **48**, 67-87.

Van den Berg, C. and Rayner, J. M. V. 1995. The moment of inertia of bird wings and the inertial power requirement for flapping flight. *J. Exp. Biol.* **198**, 1655-1664.

Wakeling, J. M. and Ellington, C. P. 1997. Dragonfly Flight. I-IV. *J. Exp. Biol*. **200**, 583-600.

Warrick, D. R. & Dial, K. P. 1998. Kinematic, aerodynamic and anatomical mechanisms in the slow, maneuvering flight of pigeons. *J Exp Bio* **201**, 655–672.

Warrick, D. R., Tobalske, B. W., & Powers, D. L. 2005 Aerodynamics of the hovering hummingbird. *Nature* **435**, 1094-1097. (DOI 10.1038/nature03647)

Webb, P. W. 2002 Kinematics of plaice, *Pleuronectes platessa*, & cod, *Gadus morhua*, swimming near the bottom. *J. Exp. Biol.* **205**: 2125-2134.

Weis-Fogh, T. 1972. Energetics of Hovering Flight in Hummingbirds and in Drosophila. *J Exp Bio* **56**, 79–104.

Welch, K. 2011 The power of feeder-mask respirometry as a method for examining hummingbird energetics. *Comp. Biochem. Physiol., Part A: Mol. Integr. Physiol*. **158**, 276-286. (DOI 10.1016/j.cbpa.2010.07.014)

Wells, D. J. 1993. Muscle Performance in Hovering Hummingbirds. *J Exp Bio* **178**, 39–57.

Williamson, M. R., Dial, K. P., & Biewener, A. A. 2001. Pectoralis muscle performance during ascending and slow level flight in mallards (*Anas platyrhynchos*). *J. Exp. Biol.* **204**, 495-507.

Withers, P. C. & Timko, P. L. 1977 The significance of ground effect to the aerodynamic cost of flight and energetics of the black skimmer (*Rhyncops nigra*). *J. Exp. Biol.* **70**, 13-26.

Wolf, L. L. 1976. Avifauna of the Cerro de la Muerte region, Costa Rica. *Am. Mus. Nat. Hist. Novit.* 2606.

Wolf, M., Ortega-Jimenez, V. M., & Dudley, R. 2013 Structure of the vortex wake in hovering Anna's hummingbirds (*Calypte anna*). *Proc. R. Soc. B* **280**, 20132391. (DOI: 10.1098/rspb.2013.2391)